

Accretion-modified Stars in Accretion Disks of Active Galactic Nuclei: Contribution to AGN disk viscosity

JUN-RONG LIU,¹ JIAN-MIN WANG,^{1,2,3} AND HUA FENG¹

¹State Key Laboratory of Particle Astrophysics, Institute of High Energy Physics, Chinese Academy of Sciences, 19B Yuquan Road, Beijing 100049, China

²School of Astronomy and Space Sciences, University of Chinese Academy of Sciences, 19A Yuquan Road, Beijing 100049, China

³National Astronomical Observatory of China, 20A Datun Road, Beijing 100020, China

ABSTRACT

It is widely believed that stellar-mass black holes (sMBHs) exist within the accretion disks of active galactic nuclei (AGN), forming a distinct population termed “accretion-modified star” (AMS). Gas from the dense disk accretes onto these AMSs, dissipating substantial gravitational energy through a mini-disk around the sMBHs, which drives powerful outflows that interact with the surrounding disk gas. In this study, we investigate two scenarios for AMS accretion: episodic Bondi explosions with hyper-Eddington accretion (Scenario A) and steady Eddington accretion (Scenario B). These outflows generate turbulence, facilitating outward angular momentum transport in the AGN disk via shock interactions and angular momentum exchange. We explore a broad parameter space-spanning the central supermassive black hole (SMBH) mass (M_p), dimensionless accretion rate ($\dot{\mathcal{M}}_p$), sMBH mass function, and spatial distribution-to calculate the effective viscosity parameter α_{AMS} . Our analysis reveals the scaling relations $\alpha_{\text{AMS}} \propto \zeta M_p^2 \dot{\mathcal{M}}_p$ for Scenario A and $\alpha_{\text{AMS}} \propto \zeta M_p^{1.5} \dot{\mathcal{M}}_p^{0.1}$ for Scenario B, where ζ denotes the ratio of total sMBH mass to the SMBH disk mass. For $\zeta = 0.01$ and $M_p = 10^8 M_\odot$, α_{AMS} ranges from $\sim 3 \times 10^{-4}$ to 0.01 (Scenario A) and $\sim 3 \times 10^{-3}$ to 0.04 (Scenario B) from the inner to outer disk regions. These results demonstrate that AMS feedback provides an efficient mechanism for angular momentum transport in AGN disks.

1. INTRODUCTION

It is well established that active galactic nuclei (AGNs) are powered by gas accretion onto center supermassive black holes (SMBHs, e.g., Salpeter 1964; Zeldovich 1964). In the accretion disk scenario (e.g., Lynden-Bell 1969; Shakura & Sunyaev 1973), gas gradually moves inward as angular momentum is transported outward through viscous stresses (Lynden-Bell & Pringle 1974). This viscosity plays a crucial role in converting gravitational energy into radiation by heating the disk gas. The origin of viscosity in AGN disks is widely attributed to turbulence, which may be driven by a variety of mechanisms, including the magnetorotational instability (MRI; Balbus & Hawley 1991; Mishra et al. 2020; Begelman 2024), gravitational instability (GI; Goodman 2003; Chen et al. 2023b) in self-gravitating regions, the Rayleigh-Taylor instability (Kaisig et al. 1992; Marshall et al. 2018), or supernova explosions (Rozyczka et al. 1995; Wang et al. 2009, 2010; Yan & Wang 2010; Moranchel-Basurto et al. 2021).

Motivated by the observation of high metallicity in broad-line regions (BLRs; Hamann & Ferland 1999) and the detection of gravitational waves (GWs) from binary black holes (BBHs) mergers involving black holes heavier than typical stellar-mass black hole (sMBH; e.g., Abbott et al. 2020a), it has been recognized that stellar objects can exist in AGN disks (Artymowicz et al. 1993; Cheng & Wang 1999; Graham et al. 2020, 2023) and bulges (Zhai et al. 2025). The evolution of stars in AGN disks leads primarily to two outcomes, an “immortal” state or runaway accretion, depending on their location in the disk and the local accretion rate (Ali-Dib & Lin 2023; Dittmann & Cantiello 2025; Fabj et al. 2025a; Xu 2025). The latter pathway produces energetic transients such as supernovae and γ -ray bursts (GRBs), leaving behind neutron stars or black holes (Li et al. 2023; She et al. 2025). In addition to in situ evolution, black holes can also be captured from the nuclear stellar cluster and enter the disk (Rowan et al. 2025; Whitehead et al. 2025a). The dense AGN disk environment provides ideal conditions for these seed black holes to grow

into the massive black holes observed in exceptional GW events, such as famous GW190521 (Abbott et al. 2020a; Graham et al. 2020), GW190814 (Abbott et al. 2020b; Yang et al. 2025), and the recent GW231123 (The LIGO Scientific Collaboration et al. 2025; Delfavero et al. 2025). When two sMBHs come sufficiently close to overcome the tidal force of the central SMBH, they form a BBH (Wang et al. 2021b; Whitehead et al. 2025b). These BBHs subsequently interact with the surrounding gas (Dittmann et al. 2025; Fabj et al. 2025b; Kishor Joshi et al. 2025), the central SMBH (Postiglione et al. 2025), and potentially a third sMBH (Fabj & Samsing 2024; Wang et al. 2025c,d; Samsing et al. 2025).

Many efforts have been made to theoretically study the properties of embedded sMBHs in AGN disks and identify their electromagnetic observational signatures. When these sMBHs orbit the central SMBH, they form extreme mass-ratio inspiral (EMRI) systems (Abhishek Hegade K. et al. 2025; Cheng et al. 2025; Duque et al. 2025; Sun et al. 2025). Applied to Sgr A*, such systems can manifest as hot spots and have successfully reproduced the observed infrared light curves and spectral energy distribution (SED, Wang et al. 2023a). In the γ -ray band, sMBHs are expected to produce GRB via relativistic jets (Zhang et al. 2024; Kang et al. 2025; Yuan & Lei 2025). Several candidate events have been reported, such as GW150914 associated with a bright γ -ray event (Tagawa et al. 2023a), GRB 191019A (Lazzati et al. 2023; Levan et al. 2023), and GW S241125n associated with a γ -ray counterpart (Zhang et al. 2025b). In optical and UV bands, the interaction between relativistic jets and the disk gas can form a jet-cocoon structure that emits thermal radiation (Chen & Dai 2025), offering a possible explanation for observed AGN optical flares (He et al. 2025). Additionally, magnetic reconnection driven by sMBHs may account for short-term AGN variability (Xing et al. 2025). In radio observations, the AGN disk environment has been invoked to explain the large dispersion measure and rotation measure of bright fast radio bursts (Zhao et al. 2024).

The sMBHs embedded in AGN disks often experience hyper-Eddington accretion, significantly exceeding typical super-Eddington accretion rates (e.g., Wang et al. 2021a,b; Liu et al. 2024; Luo & Wang 2025; Jiao et al. 2025) within the framework of Bondi accretion (Bondi 1952). This intense accretion plays a critical role in sMBH evolution, leading such objects to be referred to as “accretion-modified star” (AMS, Wang et al. 2021a). AMSs are expected to launch powerful outflows (e.g., Wang et al. 2021a; Tagawa et al. 2022; Chen et al. 2023a; Liu et al. 2024) or Blandford-Znajek jets (e.g., Wang et al. 2021b; Tagawa et al. 2023b) as mechanical feedback. These outflows or jets collide with the AGN disk, producing shocks that heat the surrounding gas and accelerate electrons to relativistic speeds (Blandford & Eichler 1987). The process gives rise to additional thermal and non-thermal emission (Wang et al. 2021a; Tagawa et al. 2023b; Liu et al. 2024), which superimpose on the intrinsic AGN radiation. For instance, collective thermal emission from AMS populations can influence the SED of the SMBH disk and may help explain the shallow spectral shape seen in quasar composite spectra (Zhou et al. 2024). Meanwhile, γ -rays originating from AMSs could be detectable in radio-quiet AGNs (Liu et al. 2025b,a), where jet-related emission is relatively subdued.

This work represents the fifth in a series of papers dedicated to exploring the behavior of black holes embedded in AGN disks (Wang et al. 2021a,b, 2023a; Liu et al. 2024). In this study, we propose a mechanism whereby outflows from AMSs facilitate outward angular momentum transport in AGN disks through momentum exchange between shocks and disk gas, a process analogous to that invoked in supernova feedback (Rozyczka et al. 1995; Moranchel-Basaruto et al. 2021). This mechanism contributes significantly to the viscosity of the AGN disk, particularly in the outer regions, and thus offers a potential solution to the long-standing low-viscosity problem. Moreover, sufficiently abundant AMS populations can heat the AGN accretion disk, alter its density and temperature profiles (Wang et al. 2025a; Epstein-Martin et al. 2025), and help maintain gravitational stability in the outer regions of a Shakura-Sunyaev disk.

The paper is organized as follows: In § 2, we describe in detail the AMS models and their feedback, including episodic accretion scenario associated with Bondi explosion (§ 2.1) and steady accretion scenario (§ 2.2). In § 3, we calculate the angular momentum transfer rate of the AGN disk driven by strong outflows and present the resulting effective viscosity parameter α_{AMS} across a typical parameter space, taking into account different sMBH mass functions and spatial distributions. In § 4, we summarize the main results and provide a general discussion. In Appendix A, we present the radial profiles of the viscosity parameter as a function of SMBH mass and accretion rate.

2. MODEL

In the context of accretion in the SMBH disk, two distinct physical scenarios are commonly discussed. The first involves the classical Eddington limit, in which isotropic radiation pressure balances gravitational forces, thus inhibiting further accretion onto the central black hole. The situation changes considerably, however, in the presence of anisotropic accretion, such as when an accretion disk forms around the black hole (e.g., Kato et al. 2008). In such a configuration, matter can accrete at rates significantly exceeding the Eddington limit, enabling not only super-Eddington but even hyper-Eddington accretion flows (e.g., Abramowicz et al. 1980; Wang et al. 2021a). In this paper, we examine both of these accretion regimes in the context of AMSs and evaluate their role in driving viscosity within AGN disk.

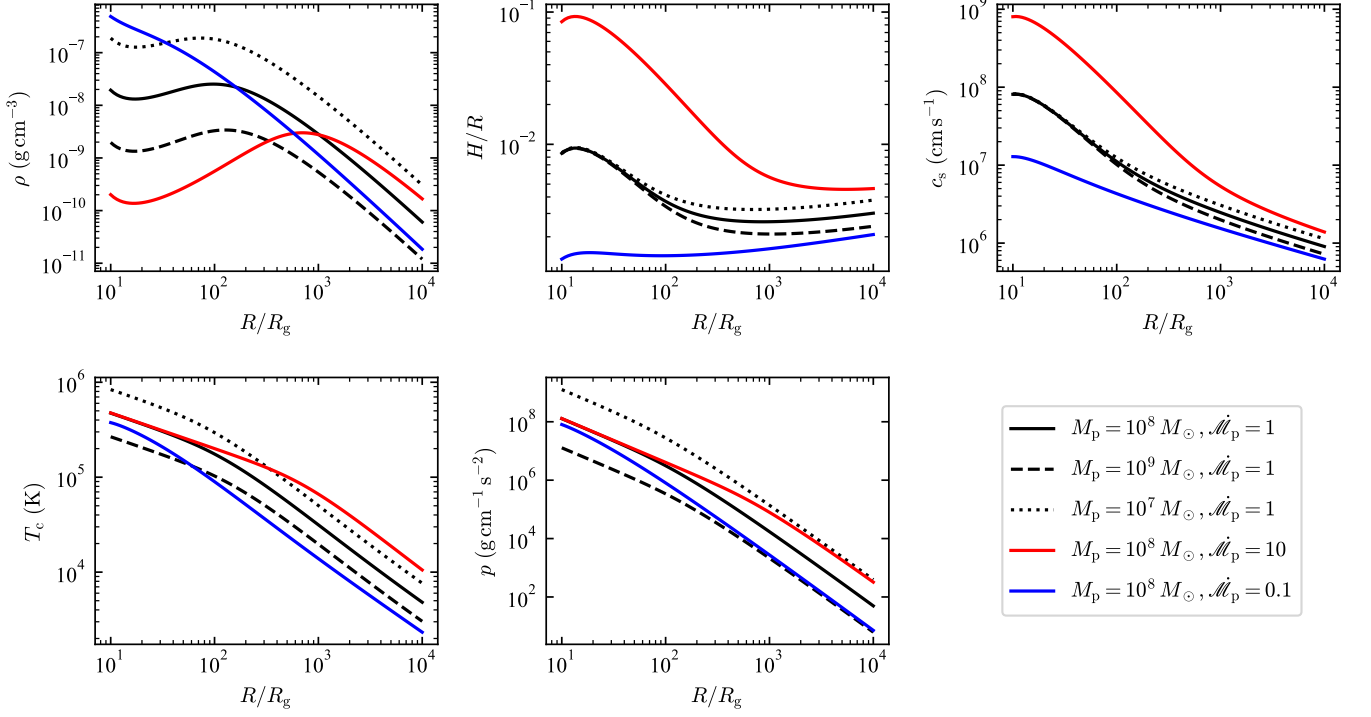


Figure 1. Radial distribution of the gas density ρ , half-thickness H , sound speed c_s , midplane temperature T_c , and total pressure p for a standard disk model, shown for different SMBH masses (M_p) and accretion rates (\dot{M}_p).

We adopt the standard disk model of Shakura & Sunyaev (1973) and investigate the viscosity contributed by outflows driven from AMSs. We consider a sMBH of mass M_s embedded in the AGN disk and orbiting a central SMBH of mass M_p with an accretion rate \dot{M}_p . Here, the subscript “p” and “s” denote “primary” and “secondary”, respectively. The dimensionless accretion rate of the SMBH is defined as $\dot{\mathcal{M}}_p \equiv \dot{M}_p c^2 / L_{\text{Edd},p}$, where $L_{\text{Edd},p} = 4\pi G M_p m_p c / \sigma_T$ is the Eddington luminosity of the SMBH, G is the gravitational constant, m_p is the proton mass, c is the speed of light, and σ_T is the Thomson scattering cross section. We explore the parameter space with $M_p = 10^7, 10^8, 10^9 M_\odot$ and $\dot{\mathcal{M}}_p = 0.1, 1, 10$. The viscosity parameter of the AGN disk is taken as $\alpha = 0.1$.

Figure 1 presents the radial profiles of density ρ , half-thickness H , sound speed c_s , midplane temperature T_c , and total pressure p for the standard accretion disk model (Shakura & Sunyaev 1973; Kato et al. 2008). It should be noted, however, that the SED of the disk could be modified when radiation from AMS is taken into account (Liu et al. 2024; Zhou et al. 2024). Furthermore, the outer disk structure may be significantly influenced if the energy released by AMS becomes comparable to the local viscous energy dissipation (Epstein-Martin et al. 2025; Wang et al. 2025b), in a manner analogous to the feedback-dominated accretion flows discussed in Gilbaum & Stone (2022). In the present study, we adopt the standard Shakura-Sunyaev disk model and neglect the feedback from AMS energy injection on the disk’s temperature and density structure. This simplification is justifiable when the total sMBH mass is substantially smaller than that of the central SMBH (see mass function of sMBHs in § 3.1) and the viscosity contributed by AMS remains below 0.1 (see result in § 3.2). However, in cases where the total sMBH mass approaches or exceeds the SMBH mass, a self-consistent “AMS-AGN disk” model would be required to reassess the structural parameters illustrated in Figure 1. The development of such a model lies beyond the scope of this paper and remains a subject for future investigation.

2.1. Scenario A: Episodic accretion for Bondi explosion

Figure 2 illustrates two types of AMS, Type I (Bondi explosion phase) and Type II (rejuvenation phase), orbiting the central SMBH in Keplerian motion within the AGN accretion disk (Wang et al. 2021b). Type I AMSs undergo hyper-Eddington accretion fueled by the dense gas of the AGN disk (e.g., Wang et al. 2021a; Chen et al. 2023a; Liu et al. 2024), producing strong outflows as a mechanical feedback (e.g., Cao & Gu 2022; Liu et al. 2024). When the outflow velocity surpasses the local sound speed, it drives shocks into the surrounding gas (e.g., Wang et al. 2021a; Liu et al. 2024). These shocks heat the gas and create a low-

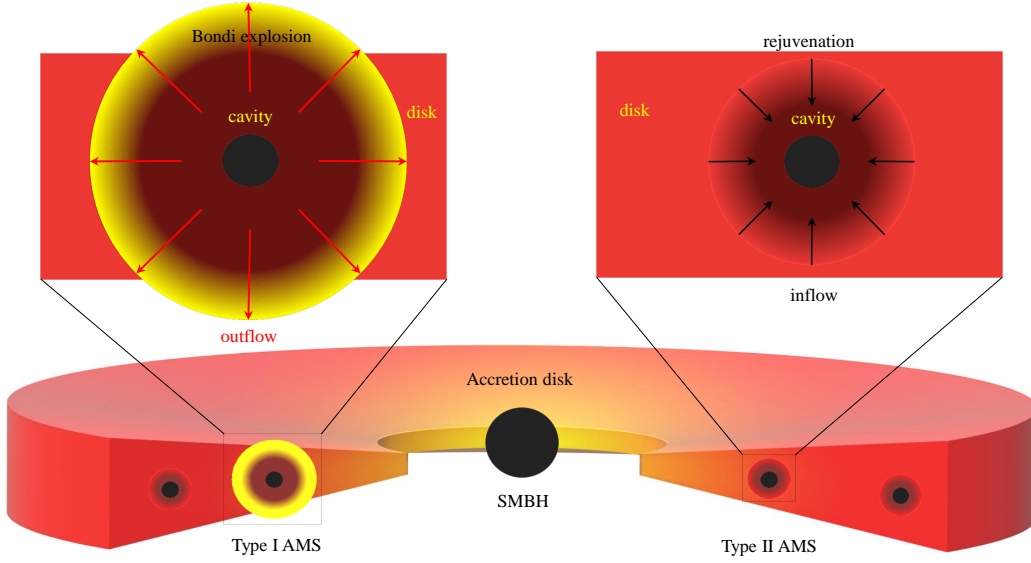


Figure 2. Schematic illustration of AMSs in an AGN accretion disk. The upper left panel depicts a Type I AMS during the Bondi explosion phase, in which a strong outflow interacts with the surrounding disk gas. The upper right panel shows a Type II AMS in the subsequent rejuvenation phase, characterized by a low-density cavity. The bottom panel illustrates the general scenario of sMBHs embedded in the dense AGN disk, accreting gas and forming AMSs. Gas density is color-coded: yellow (high), red (medium), and brown (low).

density cavity (brown region in the figure). The shocked gas radiates thermal blackbody radiation, while electrons accelerated to relativistic speeds by the shocks produce non-thermal emission via synchrotron radiation and inverse Compton scattering (Liu et al. 2024). This violent energy-release process, powered by Bondi accretion, was originally termed a “Bondi explosion” in Wang et al. (2021a) and has been adopted in their series papers. After a Type I AMS forms a cavity, the gas within it cools. Low and medium density gas from the surroundings subsequently refills the cavity under pressure, marking the rejuvenation phase (Type II AMS). During this stage, the accretion rate drops sharply and the AMS enters a low-activity state. The rejuvenation time is generally much longer than the outflow expansion timescale, so Type II AMSs dominate the lifetime of an AMS. This prevents runaway growth of sMBHs, thereby preserving the AGN disk structure. In this work, we focus primarily on the Bondi explosion process of Type I AMSs due to their significantly greater energy release compared to Type II AMSs.

We consider a sMBH corotating with the AGN disk, as shown in Figure 2. Its accretion rate is given by the Hoyle-Lyttleton-Bondi formulation (Hoyle & Lyttleton 1939; Bondi 1952), modified in thin disks (Kocsis et al. 2011),

$$\dot{M}_s = \frac{4\pi G^2 M_s^2 \rho}{(c_s^2 + \Delta v^2)^{3/2}} f_{\text{Hill}} f_{\text{H}}, \quad (1)$$

where $f_{\text{Hill}} = \min\{R_{\text{Hill}}/R_{\text{Bon}}, 1\}$ is the reduction factor due to tidal effects, $f_{\text{H}} = \min\{H/R_{\text{Bon}}, 1\}$ accounts for the limited H of the sMBH disk, and $R_{\text{Hill}} = (M_s/3M_p)^{1/3} R$ is the Hill radius of the sMBH. The Bondi radius is defined as (Edgar 2004)

$$R_{\text{Bon}} = \frac{GM_s}{c_s^2}. \quad (2)$$

We introduce the dimensionless accretion rate of the AMS as $\dot{\mathcal{M}}_s \equiv \dot{M}_s c^2 / L_{\text{Edd},s}$, where $L_{\text{Edd},s} = 4\pi GM_s m_p c / \sigma_T$ is the Eddington luminosity of the sMBH. The relative velocity between the sMBH and the surrounding gas is taken as $\Delta v = \Omega_K \times \min\{R_{\text{Bon}}, R_{\text{Hill}}\}/2$, with $\Omega_K = \sqrt{GM_p/R^3}$ being the Keplerian angular velocity. While the characteristic accretion scale in isolation is typically the Bondi radius R_{Bon} (e.g., Edgar 2004), within an AGN disk the effective accretion region is often limited by the smaller Hill radius or disk height (Kocsis et al. 2011; Liu et al. 2024).

As shown in the upper three panels of Figure 3, $H < R_{\text{Bon}}$ and $R_{\text{Hill}} < R_{\text{Bon}}$ hold in most of the parameter space, except at small disk radii ($R/R_g < 100$) and for low sMBH masses ($10M_\odot$), where $R_g = GM_p/c^2$ is the gravitational radius and M_\odot

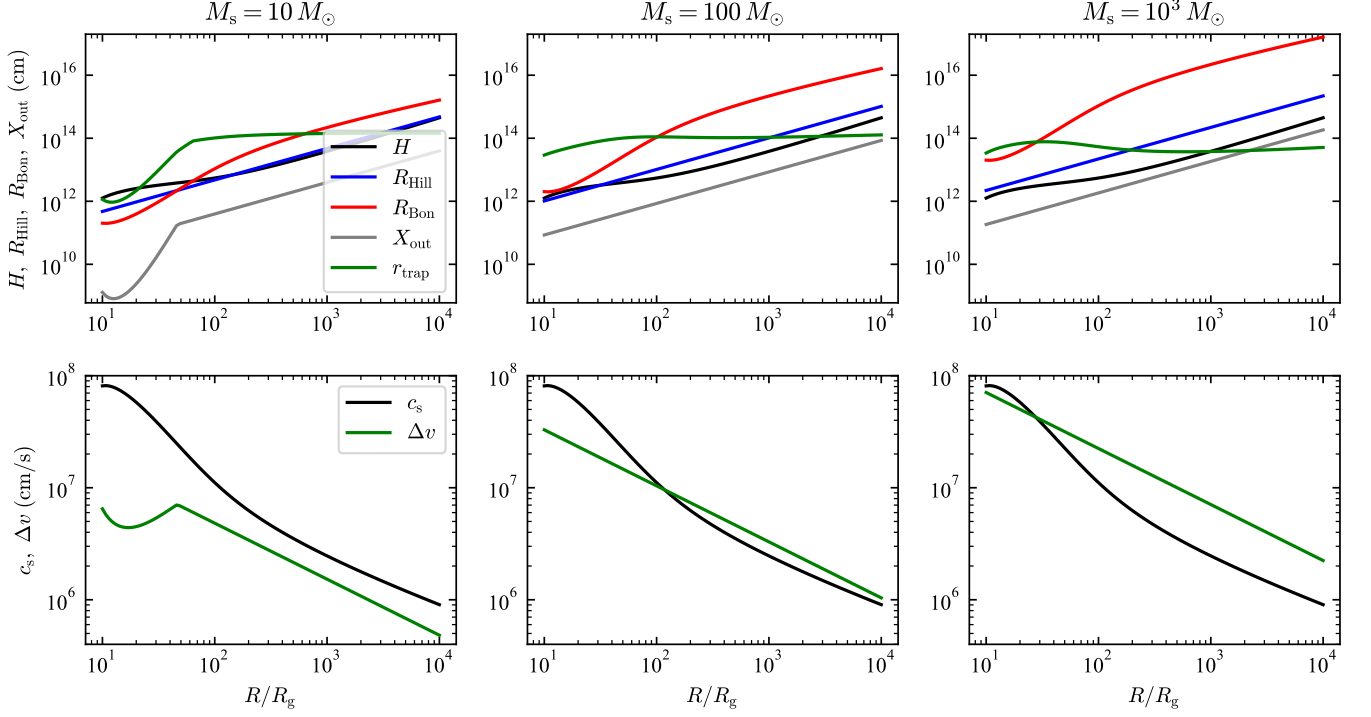


Figure 3. Top: The disk height H , the Hill radius R_{Hill} , the Bondi radius R_{Bon} , and the size of the sMBH disk X_{out} as functions of the disk radius R . Bottom: The sound speed c_s and the differential velocity Δv between the sMBH and the disk gas. The left, middle, and right panels correspond to sMBH masses of $10 M_\odot$, $100 M_\odot$, and $1000 M_\odot$, respectively. The SMBH mass and accretion rate are fixed at $M_p = 10^8 M_\odot$ and $\dot{M}_p = 1$.

denotes the solar mass. These inequalities indicate that the accretion region of an sMBH in an AGN disk is primarily constrained by two factors, i.e., geometry effect (H) and tidal effect (R_{Hill}). Even in the outer disk, where H is larger, it remains smaller than R_{Bon} , continuing to restrict the accretion regions. Although increasing M_s or R enlarges R_{Hill} , it still does not exceed R_{Bon} in most cases. Only when both R and M_s are smaller, where $R_{\text{Hill}} > R_{\text{Bon}}$ and $H > R_{\text{Bon}}$, can both geometry effect and tidal limitations be neglected. On the other hand, for more massive sMBHs in the outer disk, the accretion increasingly deviates from spherical symmetry. In addition, the differential velocity between the sMBH and the disk gas suppresses the accretion rate. The lower three panels of Figure 3 compare the relevant velocities and illustrate the resulting suppression of accretion due to this relative motion. For low-mass sMBHs ($10 M_\odot$), $c_s > \Delta v$, implying subsonic relative motion and favoring spherical Bondi accretion. In contrast, for higher sMBH masses ($R/R_g \gtrsim 100$) in the outer disk, Δv becomes comparable to or greater than c_s , particularly for $M_s = 10^3 M_\odot$. In such cases, the supersonic relative motion disrupts spherical inflow and significantly reduces \dot{M}_s .

The hyper-Eddington accretion develops outflows, with the kinetic power given by (Liu et al. 2024)

$$L_{\text{out}} = \eta_{\text{rad}} f_{\text{acc}} (1 - f_{\text{adv}}) \dot{M}_s c^2, \quad (3)$$

where $\eta_{\text{rad}} \approx 0.1$ denotes the radiative efficiency, and $f_{\text{adv}} \approx 0.9$ is the advection fraction. The value of f_{adv} is quite uncertain due to the complex interplay of advection, photon trapping, and outflow dynamics (e.g., simulations in Takeuchi et al. 2009). The factor $f_{\text{acc}} = (X_{\text{in}}/r_{\text{out}})^s$ represents the fraction of the Bondi accretion rate that ultimately reaches the sMBH, where $r_{\text{out}} = \min\{X_{\text{out}}, r_{\text{tr}}\}$ is the injection radius of the outflows, $r_{\text{tr}} = 3\dot{M}_s h r_g$ is the photon trapping radius (e.g., Kato et al. 2008; Kitaki et al. 2021), $h \sim 0.45$ is the aspect ratio of sMBH disk (see Equation (A14) in Liu et al. 2024), and $r_g = GM_s/c^2$ is the gravitational radius of the sMBH. Here, the index s , ranging from 0 to 1, depends on the ratio of the radiation energy to the dissipated gravitational energy (Begelman 2012). A moderate index of $s = 1/2$ is adopted in this work. The inner radius of the sMBH disk is taken as $X_{\text{in}} = 6 r_g$, corresponding to the innermost stable circular orbit around a Schwarzschild black hole. The outer radius $X_{\text{out}} = (\Delta R)^4 M_p / 4R^3 M_s$ is derived from angular momentum conservation of the infalling material (see Equation (A1) in Liu et al. 2024), where $\Delta R = \min\{R_{\text{Bon}}, R_{\text{Hill}}\}$ is the characteristic size of the accretion region. As shown

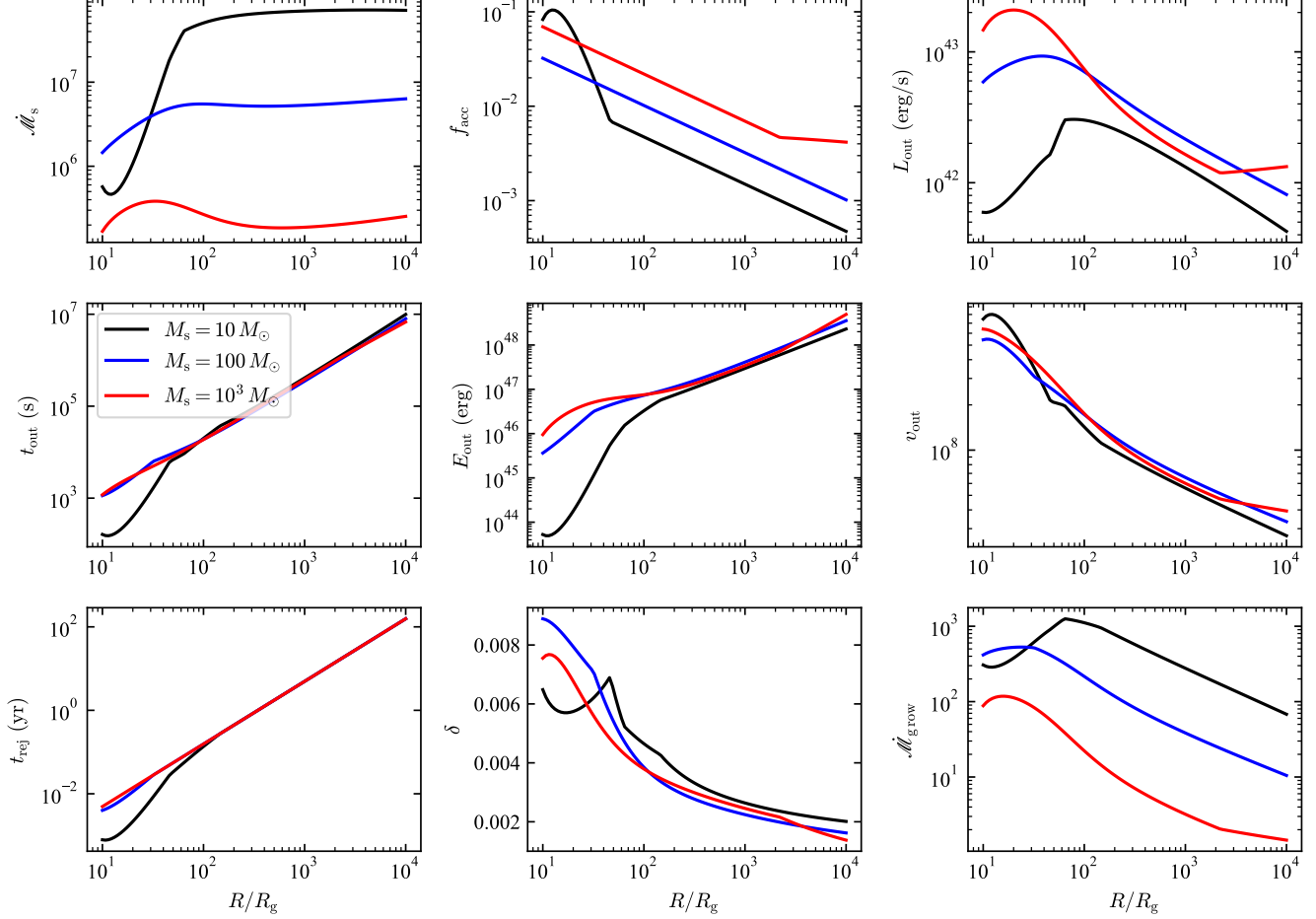


Figure 4. Radial profiles of key quantities in the Bondi explosion scenario (Scenario A), showing their variation with disk radius and sMBH mass (M_s). Quantities include \dot{M}_s (dimensionless sMBH accretion rate), f_{acc} (accretion rate fraction), L_{out} (outflow power), t_{out} (outflow expansion time), E_{out} (total outflow energy), v_{out} (outflow velocity), t_{rej} (rejuvenation time), δ (duty cycle), and \dot{M}_{grow} (net sMBH growth rate). The SMBH mass and accretion rate are fixed at $M_p = 10^8 M_\odot$ and $\dot{M}_p = 1$.

in Figure 3, X_{out} is typically an order of magnitude smaller than R_{Hill} , except for the low-mass sMBHs in the inner disk. When $R_{\text{Hill}} < R_{\text{Bon}}$, we have $\Delta R = R_{\text{Hill}}$, yielding $X_{\text{out}} = R_{\text{Hill}}/12$. This indicates that the sMBH disk remains gravitationally bound to the sMBH and is not tidally disrupted by the central SMBH. As illustrated in Figure 4, L_{out} increases with sMBH mass M_s in the inner disk. However, in the outer disk ($R/R_g \gtrsim 100$), L_{out} exhibits a non-monotonic dependence on M_s : it rises as M_s increases from 10 to $100 M_\odot$, but declines when M_s increases further to $10^3 M_\odot$. This behavior results from the suppression of spherical accretion deviation due to increased differential motion. Additionally, L_{out} decreases with disk radius R , primarily due to the rapid decline in gas density ρ .

Shocks within the Bondi radius region heat the gas and temporarily halt accretion over an accretion timescale, which corresponds to the outflow expansion timescale t_{out} . Based on the standard cavity evolution model given by Weaver et al. (1977, Equation (21)), $R(t) = (125/154\pi)^{1/5} L_{\text{out}}^{1/5} \rho^{-1/5} t^{3/5}$, the timescale t_{out} is derived as follows:

$$t_{\text{out}} = \left(\frac{231 M_{\text{out}} R_{\text{out}}^2}{250 \pi^2 L_{\text{out}}} \right)^{1/3}, \quad (4)$$

where $R_{\text{out}} = \min\{R_{\text{Bon}}, R_{\text{Hill}}, H\}$ is the radius at which infalling gas from the SMBH disk is halted by the outflow, and the mass enclosed within R_{out} is $M_{\text{out}} = 4\pi R_{\text{out}}^3 \rho/3$. The outflow can break out of the disk under certain conditions (Chen et al. 2023a); however, here we focus on its interaction with the AGN disk. The resulting turbulence is primarily constrained by R_{out} provided the overall disk structure remains intact despite the outflow. When $R_{\text{out}} = H$, this corresponds to the maximum lateral

extent of the cavity, as the outflow expands vertically but not horizontally after emerging from the disk (see upper left panel of Figure 2). If $R_{\text{out}} = R_{\text{Bon}}$ or R_{Hill} , it represents the ‘‘choking’’ radius. Additionally, the timescale t_{out} in Equation (4) differs slightly from the order-of-magnitude estimate given by Liu et al. (2024, Equation (9)) by a factor of $(231/125\pi^2)^{1/3}$. As shown in Figure 4, t_{out} increases from hours to months as the SMBH location varies from 10 to $10^4 R_g$. This trend reflects the longer time required to accumulate sufficient energy to break out of the disk at larger radii, despite the lower gas density. The kinetic energy accumulated within the region is given by

$$E_{\text{out}} = \frac{6}{11} L_{\text{out}} t_{\text{out}}, \quad (5)$$

where the factor 6/11 arises because the total injected energy is partitioned between the kinetic energy of the outflow and the internal energy of the cavity (see Equation (20) in Weaver et al. 1977). As indicated in Figure 4, E_{out} ranges from 10^{44} to 10^{49} erg. In the inner disk region, E_{out} increases noticeably with SMBH mass, consistent with stronger accretion at higher masses. In the outer disk, however, E_{out} depends only weakly on M_s but rises significantly with R . This behavior arises because the greater disk height at larger radii, together with the longer duration of Bondi accretion (t_{out}), allows more energy to accumulate before the outflow breaks out. The outflow velocity is given by

$$v_{\text{out}} = \frac{3R_{\text{out}}}{5t_{\text{out}}}, \quad (6)$$

where the factor 3/5 accounts for the non-constant expansion speed of the outflow (see Equation (21) in Weaver et al. 1977).

After a Bondi explosion, strong outflows from a Type I AMS collide with AGN disk gas, generating shocks that fragment into small-scale turbulent vortices. The resulting turbulent viscous stress transports angular momentum outward from the inner disk regions. This mechanism is analogous to the case of a supernova exploding in an AGN disk (Rozyczka et al. 1995; Moranchel-Basaruto et al. 2021). The momentum carried by the outflows is given by $P = \sqrt{2M_{\text{out}} E_{\text{out}}}$. As shown in Figures 3-5 of Rozyczka et al. (1995) and Figure 5 of Moranchel-Basaruto et al. (2021), the shocked shell is advected inward or outward over a distance of order R_{out} on the timescale of one or several orbital periods after the Bondi explosion. This process redistributes angular momentum in the disk gas through shock interaction and angular momentum exchange. When the Bondi explosion shocks interact with the disk gas, disk fluid elements facing the inner shock lose angular momentum, while those facing the outer shock gain angular momentum. The net effect is a radial transport of angular momentum from the inner disk to the outer disk. The total angular momentum transferred is approximately

$$J = \frac{\mu}{\pi} P R_{\text{out}}, \quad (7)$$

where fudge factor μ , expected to be of order unity, can be calibrated from numerical simulations (Moranchel-Basaruto et al. 2021). For simplicity, we adopt $\mu = 1$ in the following calculations. The time-averaged angular momentum transfer rate per SMBH is

$$\dot{J} = \frac{J}{t_{\text{rej}} + t_{\text{out}}}, \quad (8)$$

where $t_{\text{rej}} = R_{\text{out}}/\alpha c_s$ is the rejuvenation time, during which the gas refills the cavity (Wang et al. 2023a; Liu et al. 2024). As shown in Figure 4, t_{rej} increases from days to 100 years with increasing R , significantly longer than t_{out} (hours to months).

The powerful outflows quench the hyper-Eddington accretion, thereby preventing runaway growth of the SMBH. The time-averaged dimensionless mass growth rate (net accretion rate) is defined as $\mathcal{M}_{\text{grow}} \equiv f_{\text{acc}} \delta \mathcal{M}_s$, where $\delta \equiv t_{\text{out}}/(t_{\text{out}} + t_{\text{rej}})$ is the duty cycle. As shown in Figure 4, the duty cycle $\delta \sim 0.004 - 0.016$ indicates that most AMSs are in the rejuvenation phase. During this phase, the accretion rate onto a Type II AMS drops significantly, and the SMBH can no longer efficiently accrete the hot, low-density gas inside the cavity. In the outer disk region, $\mathcal{M}_{\text{grow}}$ decreases with increasing SMBH mass M_s , which slows logarithmic mass growth and prevents disruptive rapid accretion. This is consistent with the analytically derived average growth timescale presented in Liu et al. (2024).

2.2. Scenario B: steady accretion of Eddington limit

In Scenario B, we adopt the optically thick wind model (Meier 2012; Zhou et al. 2019), in which the outflow and inflow maintain a steady state. The wind is launched from the inner boundary and undergoes acceleration until reaching the critical radius. The kinetic power of the outflow is limited by the Eddington luminosity $L_{\text{out}} = L_{\text{Edd},s}$. As illustrated in Figure 3, the Hill radius R_{Hill} generally exceeds the disk height H , allowing the outflow to break out of the SMBH disk. The outflow velocity

at R_{Hill} can be derived from the energy equation $4\pi R_{\text{out}}^2 v_{\text{out}}^3 \rho = L_{\text{out}}$, where $R_{\text{out}} = \min\{R_{\text{Hill}}, H\}$ is the outflow radius and R_{Bon} is given by Equation (2). This yields

$$v_{\text{out}} = \left(\frac{L_{\text{out}}}{4\pi R_{\text{out}}^2 \rho} \right)^{1/3}. \quad (9)$$

The momentum flux carried by the outflow is $\dot{P} = 4\pi R_{\text{out}}^2 v_{\text{out}}^2 \rho$. Similar to Equation (7), the angular momentum transfer rate is $\dot{J} = \mu \dot{P} R_{\text{out}} / \pi$. Substituting Equation (9), we obtain

$$\dot{J} = \left(\frac{2}{\pi} \right)^{2/3} \mu L_{\text{out}}^{2/3} R_{\text{out}}^{5/3} \rho^{1/3}. \quad (10)$$

Although this formulation provides a first-order approximation, it captures the essential physics of the angular momentum transfer process. High-resolution hydrodynamic simulations will be crucial to directly model the interaction between AMS outflows and the disk gas (e.g., Zhang et al. 2025a), from which the value of μ is derived. Such simulations help clarify the microscopic transition from shock to turbulence and thereby establish a more robust physical foundation for the torque model described by \dot{J} .

3. ANGULAR MOMENTUM TRANSFER

3.1. SMBH mass function and location

The SMBH mass function remains poorly constrained. Observations of BBH mergers by LIGO/Virgo suggest a mass distribution of the form $dN/dM_s \propto M_s^{-\beta}$, with a power-law index of $\beta = 1.3_{-1.7}^{+1.4}$ (Abbott et al. 2019). Although it is uncertain whether these mergers occur in AGN disks, the observed index may overestimate the intrinsic steepness of the mass function, since mergers involving more massive progenitors are more easily detected. In dense gaseous environments such as AGN disks, accretion is expected to harden the mass function of stars (Wang et al. 2023b; Chen & Lin 2024) and black holes, shifting the index by $\Delta\beta \sim 1.3$ (Yang et al. 2019). A similar hardening effect can also result from BBH merger processes (Li et al. 2025), with the maximum SMBH mass primarily limited by the AGN disk lifetime (Xue et al. 2025). To cover a plausible range of mass function shapes, we consider $\beta = 1, 2,$ and 3 in our calculations, along with a minimum SMBH mass $M_{\text{min}} = 10M_{\odot}$ and a maximum SMBH mass $M_{\text{max}} = 10^3 M_{\odot}$.

sMBHs embedded in an AGN disk inevitably undergo orbital migration due to dynamical friction with the surrounding gas. For simplicity, we assume their spatial distribution follows a power-law form, $dN/dR \propto R^{\gamma}$, with inner and outer disk boundaries set to $R_{\text{min}} = 10R_g$ and $R_{\text{max}} = 10^4 R_g$, respectively. A value of $\gamma = 1$ corresponds to a uniform surface number density. In an α -disk, conservative inward migration of sMBHs would yield $\gamma = 1/4$ (2/5, or 5/2) in the outer, middle, or inner regions, respectively. When BBH mergers during migration are considered, γ is expected to be smaller. To cover a reasonable parameter space, we consider $\gamma = -1, 0, 1,$ and 2 . The joint mass and radial distribution of sMBHs is described by

$$\mathcal{N} \equiv \frac{dN}{dM dR} = \mathcal{N}_0 M^{-\beta} R^{\gamma}, \quad (11)$$

where \mathcal{N}_0 is the normalization constant.

The total gas mass in the SMBH disk is $M_{\text{disk}} = \int_{R_{\text{min}}}^{R_{\text{max}}} 4\pi R \rho H dR = 2.86 \times 10^6 M_{\odot}$. The total sMBH mass, M_{Tot} , is uncertain. We parameterize it as $M_{\text{Tot}} = \zeta M_{\text{disk}} = 2.86 \times 10^4 \zeta_2 M_{\text{disk},6} M_{\odot}$, where $\zeta_2 = \zeta / 10^{-2}$, and adopt $\zeta = 10^{-2}$ as a reference value, implying that sMBHs comprise about 1% of the disk mass. The normalization \mathcal{N}_0 is then derived from the condition $M_{\text{Tot}} = \int_{R_{\text{min}}}^{R_{\text{max}}} \mathcal{N} M dM dR$. We emphasize that ζ_2 here is quite uncertain. Chen & Lin (2024) estimated a population of about 10^5 massive stars in the outer unstable region of an AGN disk around a $10^8 M_{\odot}$ SMBH, considering accretion efficiency and thermal feedback. In comparison, this study adopts a conservative, lower number of sMBHs to estimate the viscosity contributed by AMSs. In reality, accretion and outflows from ordinary stars, neutron stars, and white dwarfs may also generate turbulence and enhance disk viscosity, but these are beyond the scope of this paper and left for future study.

The spatial distribution of sMBHs in AGN disks is not yet well constrained. Potential migration traps may occur at various locations: in the inner disk, at the transition radius between sub- and super-Keplerian rotation (Peng & Chen 2021); in the middle region, due to gravitational torques from the SMBH disk (Bellovary et al. 2016); or in the outer disk, through so-called ‘‘thermal torques’’ (Grishin et al. 2024; Vaccaro et al. 2025). These traps are considered likely sites for BBH mergers (Vaccaro 2025; Samsing et al. 2025). On the other hand, merged sMBHs may subsequently escape from such traps due to GW recoil kicks or gap-opening mechanisms (Gilbaum et al. 2025). In this work, we focus primarily on the general role played by AMSs in driving viscosity in AGN disks, and do not address the detailed effects of migration trapping, which we leave for future investigation.

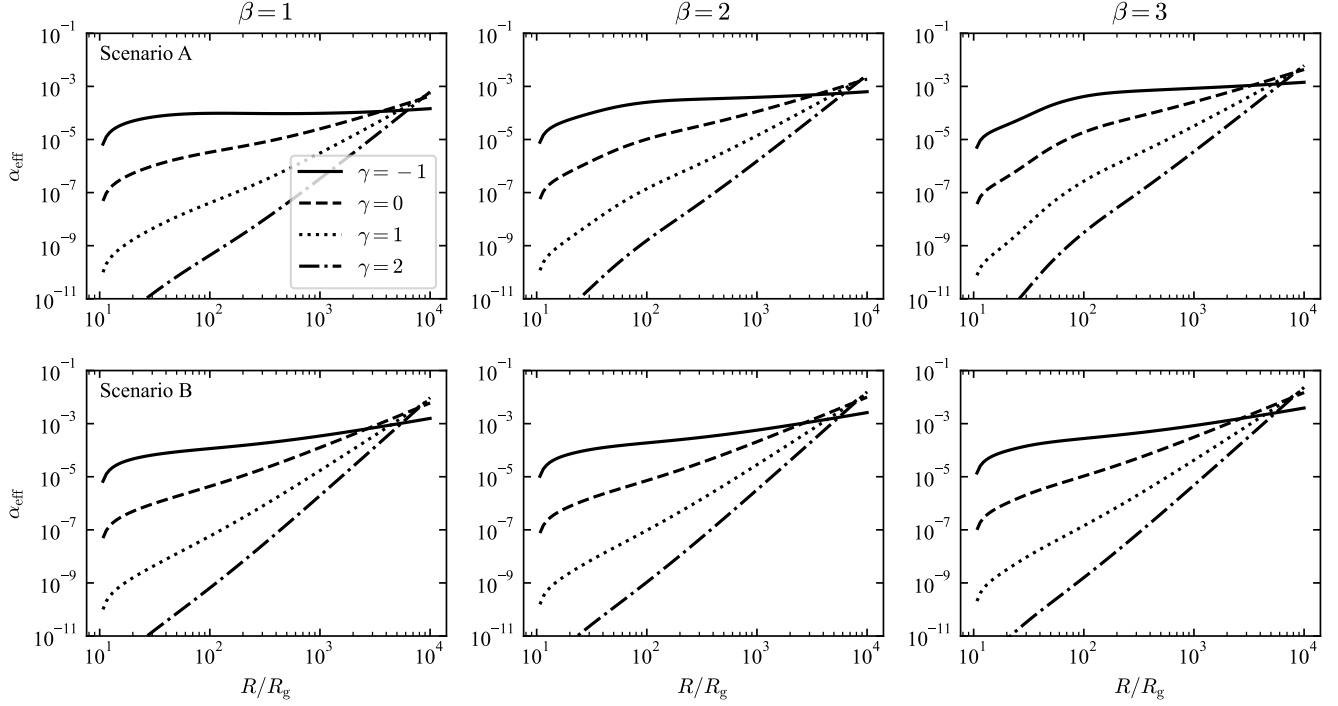


Figure 5. Radial profiles of the effective viscosity parameter α_{eff} for Scenario A (top) and B (bottom), comparing different sMBH number density distributions parameterized by β and γ . The SMBH mass and accretion rate are fixed at $M_p = 10^8 M_\odot$ and $\dot{M}_p = 1$.

3.2. effective viscosity parameter

Using Equation (8) in Scenario A, Equation (10) in Scenario B, and the sMBH distribution given in Equation (11), we derive the differential angular momentum transfer rate contributed by the entire sMBH population as a function of radius R

$$\dot{J} = \int_{M_{\min}}^{M_{\max}} \dot{J} \mathcal{N} dM. \quad (12)$$

As shown in Figure 4, the rejuvenation timescale t_{rej} ranges from $1 - 10^4$ yr, depending only weakly on the sMBH mass M_s but strongly on radius R . Since $t_{\text{out}} \ll t_{\text{rej}}$, the duty cycle δ is very small. The total viscous torque in an α -disk is $T = 2\pi R^2 \int t_{r\phi} dz = 4\pi R^2 H \alpha_{\text{eff}} p$, where the standard viscosity prescription $t_{r\phi} = \alpha_{\text{eff}} p$ is adopted (Kato et al. 2008). Applying the relation $\dot{J} = dT/dR$, the effective viscosity parameter can be expressed as

$$\alpha_{\text{eff}} = \frac{1}{4\pi R^2 H p} \int_{R_{\min}}^R \dot{J}(R') dR'. \quad (13)$$

The effective viscosity α_{eff} is directly proportional to the total sMBH mass, since $\alpha_{\text{eff}} \propto \mathcal{N}_0 \propto M_{\text{Tot}} \propto \zeta$.

In Figure 5, we compare Scenario A (Bondi explosions, top) and Scenario B (steady Eddington accretion, bottom), showing the variation of effective viscosity α_{eff} with R for different sMBH mass function exponents ($\beta = 1$ for a flat mass function, $\beta = 3$ for a steep mass function) and radial distribution exponents ($\gamma = -1$ for inner-disk concentration, $\gamma = 2$ for outer-disk concentration). In Scenario A, α_{eff} ranges from 10^{-11} to 10^{-2} from inner to outer regions. α_{eff} is small in the inner disk ($R/R_g < 100$, $10^{-11} - 10^{-4}$) and increases to $10^{-6} - 10^{-2}$ in the outer disk ($R/R_g > 10^3$). For steeper mass function ($\beta = 3$) in the outer region ($R/R_g = 10^4$), there is more low-mass sMBHs, generating more energy and turbulence consequently and leading to a larger $\alpha_{\text{eff}} \sim 10^{-2}$. Outer-disk concentration ($\gamma = 2$) increases α_{eff} in the outer disk because concentrated sMBHs inject more energy, boosting angular momentum transfer efficiency. For inner-disk concentration ($\gamma = -1$), α_{eff} is slightly dependent on the location R . In Scenario B, α_{eff} is generally slightly higher than in Scenario A. Steady outflows continuously inject energy, maintaining more stable turbulence and higher angular momentum transfer efficiency (larger \dot{P} in Equation (10), leading to larger \dot{J}). α_{eff} has a similar dependence on the mass function and the position distribution as Scenario A. In total, α_{eff}

Table 1. The global effective viscosity α_{AMS} for $M_{\text{p}} = 10^8 M_{\odot}$ and $\dot{\mathcal{M}}_{\text{p}} = 1$.

	Scenario A			Scenario B		
	$\beta = 1$	$\beta = 2$	$\beta = 3$	$\beta = 1$	$\beta = 2$	$\beta = 3$
$\gamma = -1$	0.0003	0.0011	0.0025	0.0027	0.0045	0.0067
$\gamma = 0$	0.0008	0.0033	0.0075	0.0104	0.0173	0.0257
$\gamma = 1$	0.0010	0.0042	0.0096	0.0144	0.0238	0.0354
$\gamma = 2$	0.0011	0.0047	0.0106	0.0165	0.0272	0.0405

Table 2. The same as Table 1 but for $M_{\text{p}} = 10^7 M_{\odot}$ and $M_{\text{p}} = 10^9 M_{\odot}$.

	$M_{\text{p}} = 10^7 M_{\odot}, \dot{\mathcal{M}}_{\text{p}} = 1$						$M_{\text{p}} = 10^9 M_{\odot}, \dot{\mathcal{M}}_{\text{p}} = 1$					
	Scenario A			Scenario B			Scenario A			Scenario B		
	$\beta = 1$	$\beta = 2$	$\beta = 3$	$\beta = 1$	$\beta = 2$	$\beta = 3$	$\beta = 1$	$\beta = 2$	$\beta = 3$	$\beta = 1$	$\beta = 2$	$\beta = 3$
$\gamma = -1$	0.000002	0.000011	0.000026	0.00009	0.00015	0.00023	0.022	0.068	0.119	0.08	0.13	0.20
$\gamma = 0$	0.000008	0.000034	0.000079	0.00036	0.00059	0.00088	0.066	0.201	0.350	0.30	0.50	0.75
$\gamma = 1$	0.000010	0.000044	0.000102	0.00049	0.00082	0.00121	0.084	0.252	0.432	0.42	0.69	1.03
$\gamma = 2$	0.000011	0.000049	0.000113	0.00056	0.00093	0.00139	0.092	0.275	0.469	0.48	0.79	1.18

in both scenarios covers the viscosity range required for AGN disks if a larger ζ value is adopted. This confirms AMS as a critical viscosity source alongside MRI and GI.

The total angular momentum transfer rate from the SMBH population is given by $\dot{\mathcal{J}}_{\text{tot}} = \int_{R_{\text{min}}}^{R_{\text{max}}} \dot{\mathcal{J}} dR$, while the total angular momentum of the SMBH disk is $\mathcal{J}_{\text{tot}} = \int_{R_{\text{min}}}^{R_{\text{max}}} 2\pi R^3 \Sigma \Omega dR$. The migration timescale driven by AMS feedback is then $t_{\text{mig}} = \mathcal{J}_{\text{tot}} / \dot{\mathcal{J}}_{\text{tot}}$. For a standard α disk, the viscosity timescale is $t_{\text{vis}} = (R/H)^2 / \alpha \Omega_{\text{K}}$ (Kato et al. 2008). Equating these timescales yields the global effective viscosity parameter as

$$\alpha_{\text{AMS}} \equiv \frac{\dot{\mathcal{J}}_{\text{Tot}}}{\Omega_{\text{m}} \mathcal{J}_{\text{Tot}}} \left(\frac{R_{\text{max}}}{H_{\text{max}}} \right)^2, \quad (14)$$

where $\Omega_{\text{m}}, H_{\text{max}}$ is the angular velocity and SMBH disk height at radius R_{max} , respectively. The resulting values of α_{AMS} are listed in Table 1, ranging from 3×10^{-4} to 10^{-2} for Scenario A and from 2.7×10^{-3} to 4.1×10^{-2} for Scenario B. Additionally, Table 2 provides α_{AMS} for different SMBH mass ($M_{\text{p}} = 10^7$ and $10^9 M_{\odot}$), with the corresponding results plotted in Figure 6. The results are consistent with scaling relations of $\alpha_{\text{AMS}} \propto M_{\text{p}}^2$ for Scenario A and $\alpha_{\text{AMS}} \propto M_{\text{p}}^{1.5}$ for Scenario B. Similarly, Table 3 lists α_{AMS} for different SMBH accretion rate ($\dot{\mathcal{M}}_{\text{p}} = 0.1$ and 10), as shown in Figure 7. These follow the relations $\alpha_{\text{AMS}} \propto \dot{\mathcal{M}}_{\text{p}}$ for Scenario A and $\alpha_{\text{AMS}} \propto \dot{\mathcal{M}}_{\text{p}}^{0.1}$ for Scenario B. The above scaling relations are primarily determined by variations of the disk height H and the Hill radius with M_{p} and $\dot{\mathcal{M}}_{\text{p}}$. Further details of the radial profiles are provided in Appendix A. It is noteworthy that α_{AMS} exceeds 0.1 in most cases for $M_{\text{p}} = 10^9 M_{\odot}$, where a self-consistent solution of AMS-AGN disk becomes necessary. But this extreme scenario lies beyond the scope of the present study. Through multiple iterations, a value of $\alpha_{\text{AMS}} \sim 0.1 - 1$ can be preliminarily anticipated. A more detailed investigation, particularly for systems with higher SMBH and sMBH masses, remains a subject for future work.

4. CONCLUSION AND DISCUSSION

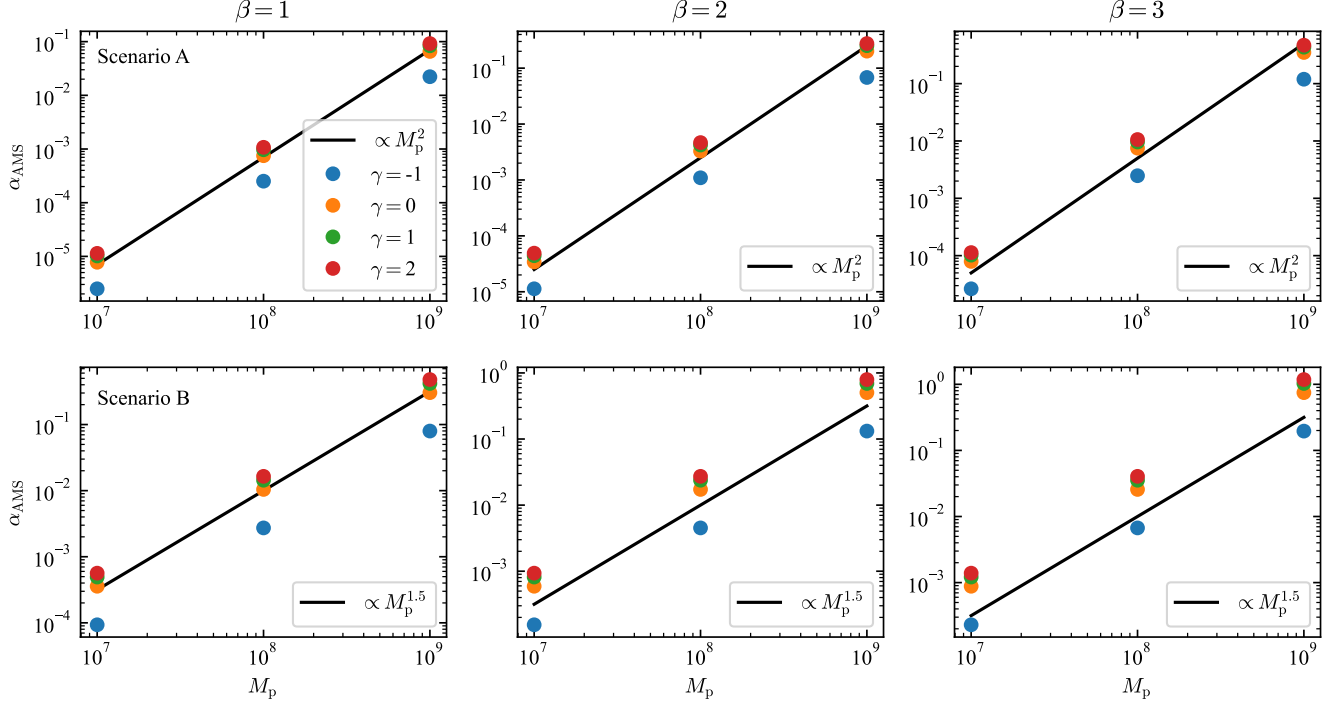


Figure 6. Global effective viscosity α_{AMS} as a function of M_p for Scenario A (top) and B (bottom). The cases for different sMBH number density distributions in the parameter space of β and γ are compared. Corresponding numerical values are listed in Tables 1 and 2.

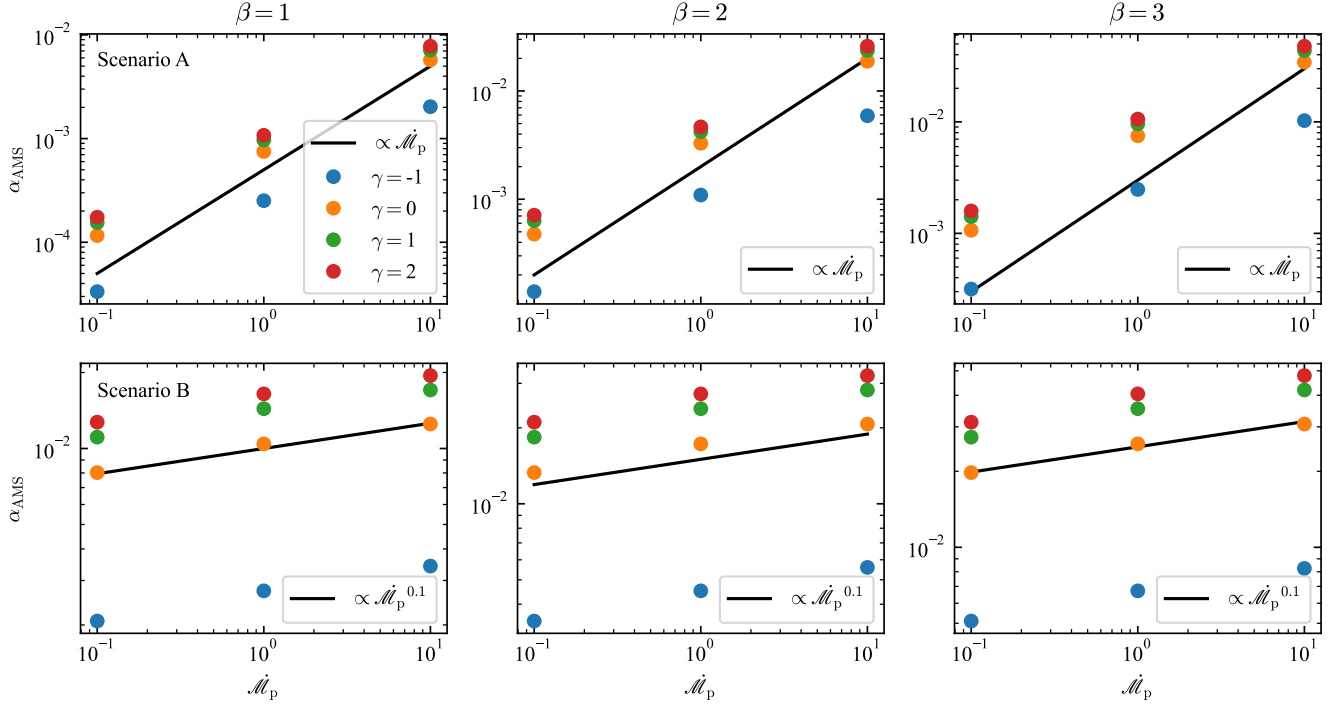


Figure 7. Global effective viscosity α_{AMS} as a function of \dot{M}_p for Scenario A (top) and B (bottom). The cases for different sMBH number density distributions in the parameter space of β and γ are compared. Corresponding numerical values are listed in Tables 1 and 3.

Table 3. The same as Table 1 but for $\dot{\mathcal{M}}_p = 0.1$ and $\dot{\mathcal{M}}_p = 10$.

	$M_p = 10^8 M_\odot, \dot{\mathcal{M}}_p = 0.1$						$M_p = 10^8 M_\odot, \dot{\mathcal{M}}_p = 10$					
	Scenario A			Scenario B			Scenario A			Scenario B		
	$\beta = 1$	$\beta = 2$	$\beta = 3$	$\beta = 1$	$\beta = 2$	$\beta = 3$	$\beta = 1$	$\beta = 2$	$\beta = 3$	$\beta = 1$	$\beta = 2$	$\beta = 3$
$\gamma = -1$	0.00003	0.00014	0.00032	0.0021	0.0034	0.0051	0.002	0.006	0.010	0.003	0.006	0.008
$\gamma = 0$	0.00012	0.00048	0.00107	0.0080	0.0133	0.0198	0.006	0.019	0.034	0.013	0.021	0.031
$\gamma = 1$	0.00015	0.00063	0.00141	0.0111	0.0184	0.0273	0.007	0.024	0.044	0.017	0.028	0.042
$\gamma = 2$	0.00017	0.00071	0.00159	0.0127	0.0211	0.0313	0.008	0.026	0.048	0.019	0.032	0.048

We studied AMS dynamical evolution and viscosity contributions in AGN disks. Two kinds of outflows, episodic outflows driven by Bondi explosion (Scenario A) and steady outflows under Eddington limit (Scenario B), lead to turbulence through the shock interaction with the AGN disk gas. This turbulence facilitates outward angular momentum transport in the disk. By comparing the migration timescale with the viscous timescale, we computed the global effective viscosity parameter α_{AMS} , which ranges from 3×10^{-4} to 10^{-2} for Scenario A and from 2.7×10^{-3} to 4.1×10^{-2} for Scenario B. In most sMBH spatial distributions, the viscosity contributed by sMBHs is higher in the outer disk regions and lower in the inner regions.

For Scenario A, AMSs exhibit biphasic evolution, alternating between Type I (Bondi explosion, t_{out} : hours to months) and Type II (rejuvenation, t_{rej} : $10^{-2} - 10^2$ years) state, with a duty cycle of $\delta \approx 0.002 - 0.009$. This process results in a net dimensionless sMBH growth rate of $\dot{\mathcal{M}}_{\text{grow}} = 1 - 10^3$, which provides seed black holes for gravitational wave (GW) events with large masses while preventing excessive sMBH growth. The sMBH accretion regions are confined by the disk height H and the Hill radius R_{Hill} , where $H < R_{\text{Bon}}$ and $R_{\text{Hill}} < R_{\text{Bon}}$ in most regions. In the outer disk, $\Delta v > c_s$ suppresses spherical accretion, thereby reducing the sMBH accretion rate $\dot{\mathcal{M}}_s$. Both Scenario A and Scenario B yield α_{AMS} values covering the required AGN disk viscosity range. The effective viscosity in the outer disk is 2-4 orders of magnitude higher than in the inner disk, indicating that AMS dominates viscosity in the outer regions. A steep sMBH mass function ($\beta = 3$) combined with outer-disk concentration ($\gamma = 2$) can raise the effective viscosity to $\alpha_{\text{eff}} \gtrsim 0.1$ in the outer disk. Conversely, a flat mass function ($\beta = 1$) and inner-disk concentration ($\gamma = -1$) lead to lower α_{eff} values. This confirms that the sMBH population distribution is a key regulator of viscosity in AGN disks.

The present model assumes power-law distributions for the sMBH population: $dN/dM_s \propto M_s^{-\beta}$ in mass and $dN/dR \propto R^\gamma$ in radius. However, “migration traps”, such as the transition zone between sub- and super-Keplerian rotation in the inner disk (Peng & Chen 2021), or regions dominated by thermal torques in the outer disk (Grishin et al. 2024), are known to exist in AGN disks and may cause sMBHs to accumulate at specific radii (e.g., $R \approx 10^4 R_g$, Trani & Di Cintio 2025). Future high-resolution N -body simulations are needed to refine the distribution function, and are expected to shift the peak location of α_{eff} seen in Figure 5. Gravitational-wave observations will provide key constraints on these model parameters (e.g., Ford & McKernan 2025; McKernan et al. 2025). While ground-based detectors LIGO/Virgo can search for binary black hole (BBH) mergers in AGN disks, the mHz band accessible to space-based detectors like Laser Interferometer Space Antenna (LISA, Babak et al. 2017), Taiji (Hu & Wu 2017), and Tianqin (Luo et al. 2016) will be particularly suited to detecting EMRIs (Wang et al. 2023a) and intermediate-mass binary black hole merger events (Dutta Roy et al. 2025). These multi-band GW observations will help determine the values of \mathcal{N}_0 , β , and γ , offering an empirical test for the theoretical predictions of α_{eff} .

¹ We thank Yi-Lin Wang for useful discussions and the anonymous referee for useful comments. We acknowledge funding support
² from the National Natural Science Foundation of China under the grant Nos. 12333003, 12025301, the National Key R&D
³ Program of China (2021YFA1600404), and the Strategic Priority Research Program of the Chinese Academy of Sciences. This
⁴ work is supported by the China Postdoctoral Science Foundation under Grant Number 2025M783227.

A. EFFECTIVE VISCOSITY VS. SMBH MASS AND ACCRETION RATE

We examine the influence of SMBH mass M_p and accretion rate \dot{M}_p on the effective viscosity α_{eff} contributed by AMSs by plotting its radial profile under different disk parameters in Figures A1-A4. The parameter sets are as follows: Figure A1 adopts $M_p = 10^9 M_\odot$ and $\dot{M}_p = 1$, Figure A2 uses $M_p = 10^7 M_\odot$ and $\dot{M}_p = 1$, Figure A3 corresponds to $M_p = 10^8 M_\odot$ and $\dot{M}_p = 10$, and Figure A4 employs $M_p = 10^8 M_\odot$ and $\dot{M}_p = 0.1$. All figures show that α_{eff} is significantly larger in the outer disk ($R/R_g > 10^3$) than in the inner disk ($R/R_g < 100$), supporting the conclusion that AMS serves as the source of viscosity in the outer disk for wide parameter space of M_p or \dot{M}_p .

In Scenario A, for Figure A1 where $M_p = 10^9 M_\odot$, α_{eff} is generally about two orders of magnitude greater than that in Figure 5. Although gas density ρ decreases, both the disk height H and the Hill radius R_{Hill} increase, leading to more energy release (see Equation 1). Conversely, in Figure A2 with $M_p = 10^7 M_\odot$, α_{eff} is roughly two orders of magnitude smaller. This supports the scaling $\alpha_{\text{eff}} \propto M_p^2$ as can be seen in Figure 6. In Figure A3 with $\dot{M}_p = 10$, the higher ρ and larger H enhance the AMS outflow strength (Equation 1), raising α_{eff} by about an order of magnitude in the outer disk compared to Figure 5. In the inner region, however, α_{eff} drops sharply due to decreasing ρ and increasing sound speed c_s . For Figure A4 with $\dot{M}_p = 0.1$, lower ρ and smaller H weaken AMS outflows, reducing α_{eff} by approximately one order of magnitude relative to Figure 5. A rough proportionality $\alpha_{\text{eff}} \propto \dot{M}_p$ is found (also see Figure 7).

In Scenario B, we find $\alpha_{\text{eff}} \propto M_p^{1.5}$ as can be seen in Figure 6, as both H and R_{Hill} increase with M_p , enhancing the angular momentum transfer rate (see Equation 10). In contrast, $\alpha_{\text{eff}} \propto \dot{M}_p^{0.1}$ shows almost no variation with the SMBH accretion rate (also see Figure 7), since R_{Hill} is independent of \dot{M}_p and $H \propto \dot{M}_p^{3/20}$ is only weakly sensitive to \dot{M}_p in the outer region.

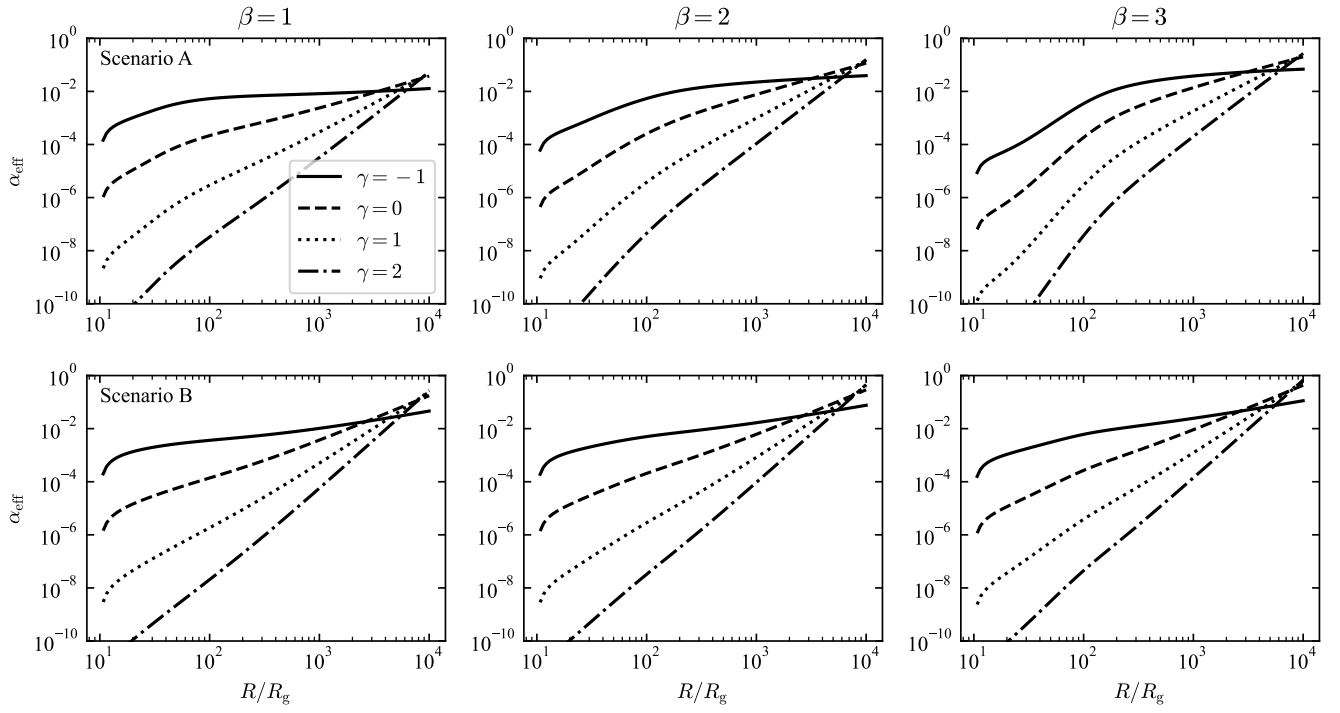


Figure A1. The same as Figure 5 but for $M_p = 10^9 M_\odot$.

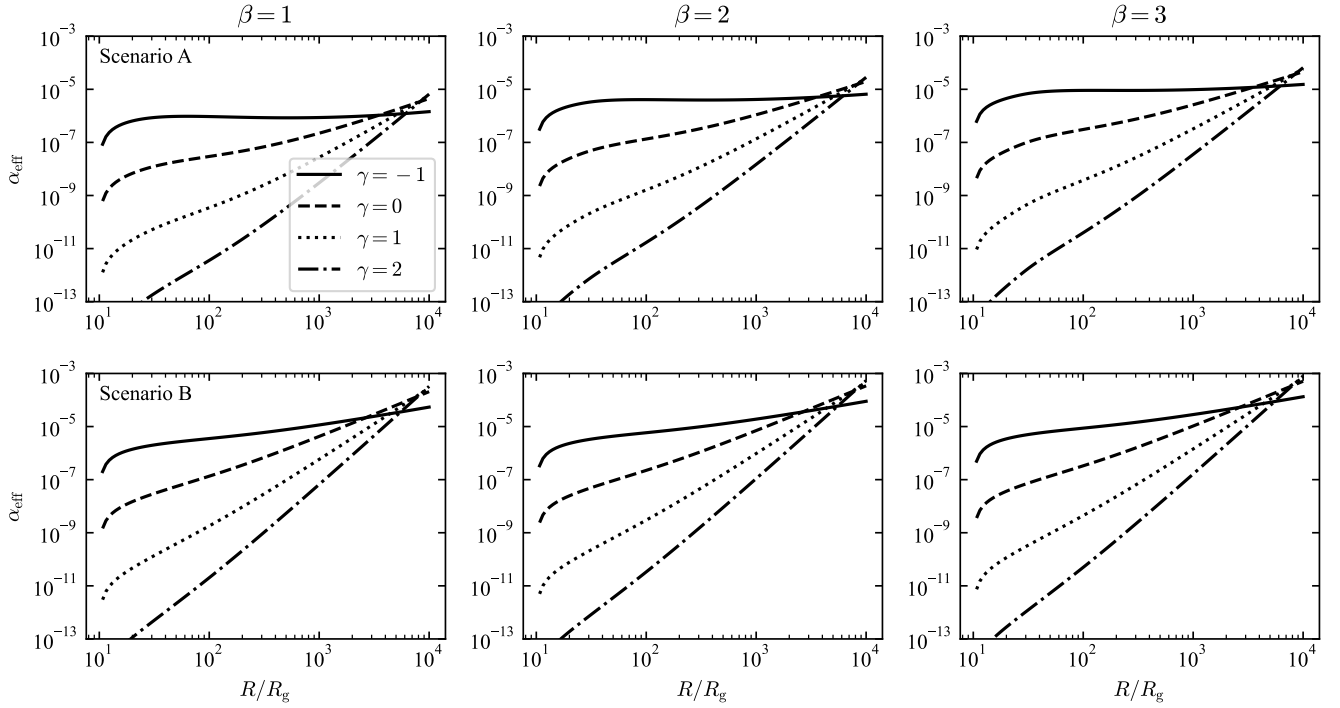


Figure A2. The same as Figure 5 but for $M_p = 10^7 M_\odot$.

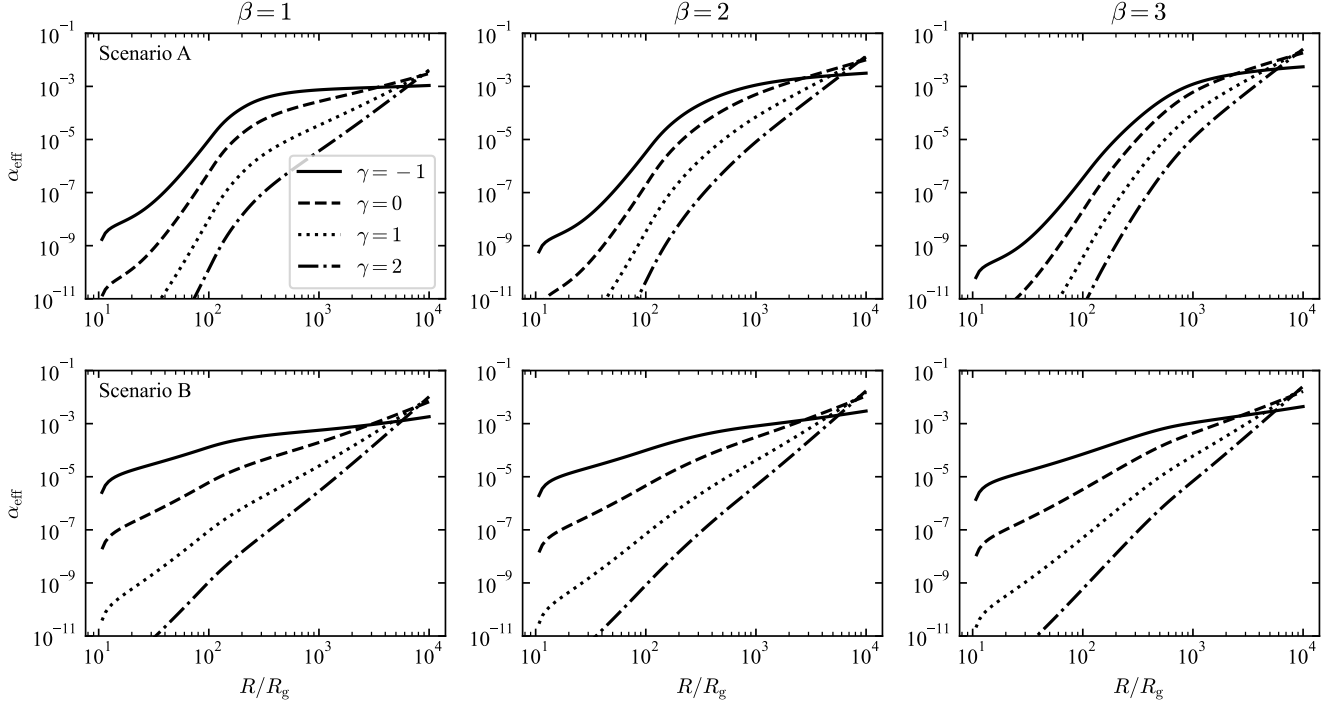


Figure A3. The same as Figure 5 but for $\dot{M}_p = 10$.

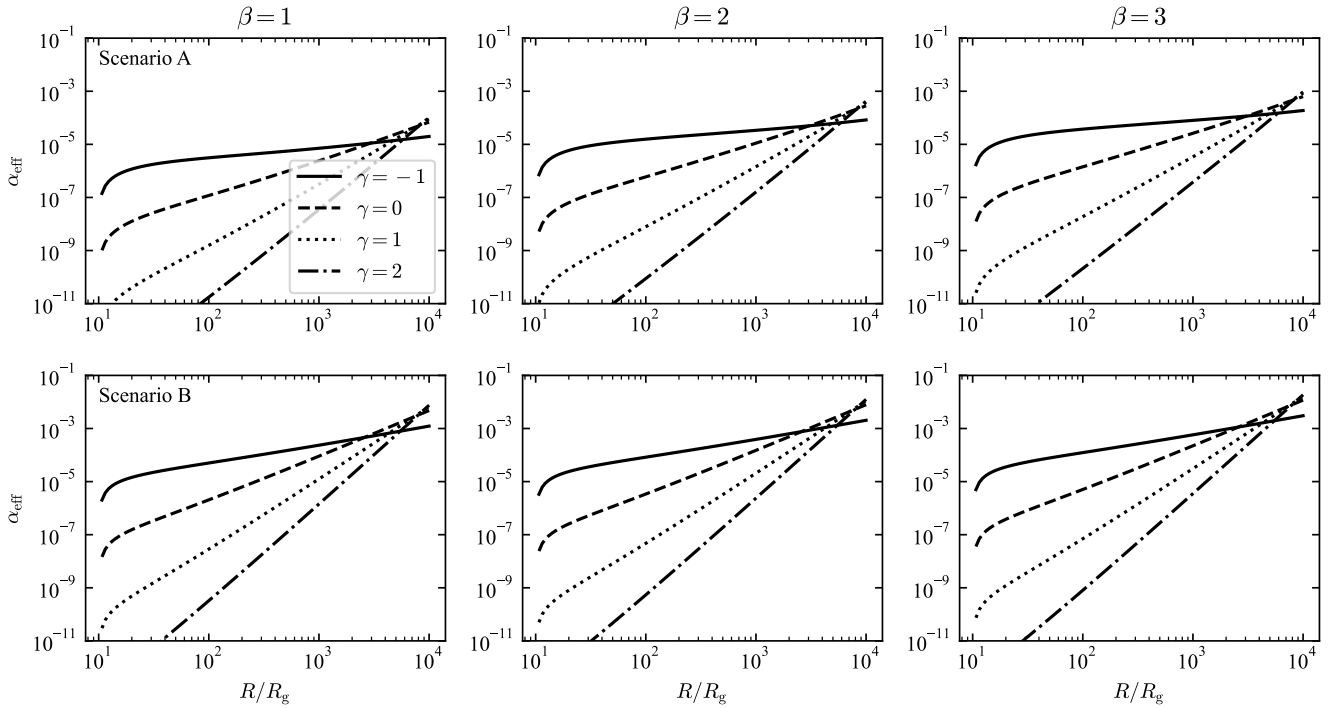


Figure A4. The same as Figure 5 but for $\dot{M}_p = 0.1$.

REFERENCES

- Abbott, B. P., Abbott, R., Abbott, T. D., et al. 2019, *ApJL*, 882, L24, doi: [10.3847/2041-8213/ab3800](https://doi.org/10.3847/2041-8213/ab3800)
- Abbott, R., Abbott, T. D., Abraham, S., et al. 2020a, *PhRvL*, 125, 101102, doi: [10.1103/PhysRevLett.125.101102](https://doi.org/10.1103/PhysRevLett.125.101102)
- . 2020b, *ApJL*, 896, L44, doi: [10.3847/2041-8213/ab960f](https://doi.org/10.3847/2041-8213/ab960f)
- Abhishek Hegade K., R., Gammie, C. F., & Yunes, N. 2025, arXiv e-prints, arXiv:2510.03564, doi: [10.48550/arXiv.2510.03564](https://doi.org/10.48550/arXiv.2510.03564)
- Abramowicz, M. A., Calvani, M., & Nobili, L. 1980, *ApJ*, 242, 772, doi: [10.1086/158512](https://doi.org/10.1086/158512)
- Ali-Dib, M., & Lin, D. N. C. 2023, *MNRAS*, 526, 5824, doi: [10.1093/mnras/stad2774](https://doi.org/10.1093/mnras/stad2774)
- Artymowicz, P., Lin, D. N. C., & Wampler, E. J. 1993, *ApJ*, 409, 592, doi: [10.1086/172690](https://doi.org/10.1086/172690)
- Babak, S., Gair, J., Sesana, A., et al. 2017, *PhRvD*, 95, 103012, doi: [10.1103/PhysRevD.95.103012](https://doi.org/10.1103/PhysRevD.95.103012)
- Balbus, S. A., & Hawley, J. F. 1991, *ApJ*, 376, 214, doi: [10.1086/170270](https://doi.org/10.1086/170270)
- Begelman, M. C. 2012, *MNRAS*, 420, 2912, doi: [10.1111/j.1365-2966.2011.20071.x](https://doi.org/10.1111/j.1365-2966.2011.20071.x)
- . 2024, *MNRAS*, 534, 3144, doi: [10.1093/mnras/stae2305](https://doi.org/10.1093/mnras/stae2305)
- Bellovary, J. M., Mac Low, M.-M., McKernan, B., & Ford, K. E. S. 2016, *ApJL*, 819, L17, doi: [10.3847/2041-8205/819/2/L17](https://doi.org/10.3847/2041-8205/819/2/L17)
- Blandford, R., & Eichler, D. 1987, *PhR*, 154, 1, doi: [10.1016/0370-1573\(87\)90134-7](https://doi.org/10.1016/0370-1573(87)90134-7)
- Bondi, H. 1952, *MNRAS*, 112, 195, doi: [10.1093/mnras/112.2.195](https://doi.org/10.1093/mnras/112.2.195)
- Cao, X., & Gu, W.-M. 2022, *ApJ*, 936, 141, doi: [10.3847/1538-4357/ac8980](https://doi.org/10.3847/1538-4357/ac8980)
- Chen, K., & Dai, Z.-G. 2025, *ApJ*, 987, 214, doi: [10.3847/1538-4357/addb48](https://doi.org/10.3847/1538-4357/addb48)
- Chen, K., Ren, J., & Dai, Z.-G. 2023a, *ApJ*, 948, 136, doi: [10.3847/1538-4357/acc45f](https://doi.org/10.3847/1538-4357/acc45f)
- Chen, Y.-X., Jiang, Y.-F., Goodman, J., & Ostriker, E. C. 2023b, *ApJ*, 948, 120, doi: [10.3847/1538-4357/acc023](https://doi.org/10.3847/1538-4357/acc023)
- Chen, Y.-X., & Lin, D. N. C. 2024, *ApJ*, 967, 88, doi: [10.3847/1538-4357/ad3c3a](https://doi.org/10.3847/1538-4357/ad3c3a)
- Cheng, K. S., & Wang, J.-M. 1999, *ApJ*, 521, 502, doi: [10.1086/307572](https://doi.org/10.1086/307572)
- Cheng, Y.-Z., Cao, Y., & Tang, Y. 2025, *PhRvD*, 111, 083010, doi: [10.1103/PhysRevD.111.083010](https://doi.org/10.1103/PhysRevD.111.083010)
- Delfavero, V., Ray, S., Cook, H. E., et al. 2025, arXiv e-prints, arXiv:2508.13412, doi: [10.48550/arXiv.2508.13412](https://doi.org/10.48550/arXiv.2508.13412)
- Dittmann, A. J., & Cantiello, M. 2025, *ApJ*, 979, 245, doi: [10.3847/1538-4357/ad9e92](https://doi.org/10.3847/1538-4357/ad9e92)
- Dittmann, A. J., Dempsey, A. M., & Li, H. 2025, *ApJ*, 990, 137, doi: [10.3847/1538-4357/adea72](https://doi.org/10.3847/1538-4357/adea72)
- Duque, F., Sberna, L., Spiers, A., & Vicente, R. 2025, arXiv e-prints, arXiv:2510.02433, doi: [10.48550/arXiv.2510.02433](https://doi.org/10.48550/arXiv.2510.02433)
- Dutta Roy, P., Mahapatra, P., Samajdar, A., & Arun, K. G. 2025, *PhRvD*, 111, 104047, doi: [10.1103/PhysRevD.111.104047](https://doi.org/10.1103/PhysRevD.111.104047)
- Edgar, R. 2004, *NewAR*, 48, 843, doi: [10.1016/j.newar.2004.06.001](https://doi.org/10.1016/j.newar.2004.06.001)
- Epstein-Martin, M., Tagawa, H., Haiman, Z., & Perna, R. 2025, *MNRAS*, 537, 3396, doi: [10.1093/mnras/staf237](https://doi.org/10.1093/mnras/staf237)
- Fabj, G., Dittmann, A. J., Cantiello, M., Perna, R., & Samsing, J. 2025a, *ApJ*, 981, 16, doi: [10.3847/1538-4357/ada896](https://doi.org/10.3847/1538-4357/ada896)
- Fabj, G., & Samsing, J. 2024, *MNRAS*, 535, 3630, doi: [10.1093/mnras/stae2499](https://doi.org/10.1093/mnras/stae2499)
- Fabj, G., Tiede, C., Rowan, C., Pessah, M., & Samsing, J. 2025b, arXiv e-prints, arXiv:2510.07952, doi: [10.48550/arXiv.2510.07952](https://doi.org/10.48550/arXiv.2510.07952)
- Ford, K. E. S., & McKernan, B. 2025, arXiv e-prints, arXiv:2506.08801, doi: [10.48550/arXiv.2506.08801](https://doi.org/10.48550/arXiv.2506.08801)
- Gilbaum, S., Grishin, E., Stone, N. C., & Mandel, I. 2025, *ApJL*, 982, L13, doi: [10.3847/2041-8213/adb7dc](https://doi.org/10.3847/2041-8213/adb7dc)
- Gilbaum, S., & Stone, N. C. 2022, *ApJ*, 928, 191, doi: [10.3847/1538-4357/ac4ded](https://doi.org/10.3847/1538-4357/ac4ded)
- Goodman, J. 2003, *MNRAS*, 339, 937, doi: [10.1046/j.1365-8711.2003.06241.x](https://doi.org/10.1046/j.1365-8711.2003.06241.x)
- Graham, M. J., Ford, K. E. S., McKernan, B., et al. 2020, *PhRvL*, 124, 251102, doi: [10.1103/PhysRevLett.124.251102](https://doi.org/10.1103/PhysRevLett.124.251102)
- Graham, M. J., McKernan, B., Ford, K. E. S., et al. 2023, *ApJ*, 942, 99, doi: [10.3847/1538-4357/aca480](https://doi.org/10.3847/1538-4357/aca480)
- Grishin, E., Gilbaum, S., & Stone, N. C. 2024, *MNRAS*, 530, 2114, doi: [10.1093/mnras/stae828](https://doi.org/10.1093/mnras/stae828)
- Hamann, F., & Ferland, G. 1999, *ARA&A*, 37, 487, doi: [10.1146/annurev.astro.37.1.487](https://doi.org/10.1146/annurev.astro.37.1.487)
- He, L., Liu, Z.-Y., Niu, R., et al. 2025, arXiv e-prints, arXiv:2507.20232, doi: [10.48550/arXiv.2507.20232](https://doi.org/10.48550/arXiv.2507.20232)
- Hoyle, F., & Lyttleton, R. A. 1939, *Proceedings of the Cambridge Philosophical Society*, 35, 405, doi: [10.1017/S0305004100021150](https://doi.org/10.1017/S0305004100021150)
- Hu, W.-R., & Wu, Y.-L. 2017, *National Science Review*, 4, 685, doi: [10.1093/nsr/nwx116](https://doi.org/10.1093/nsr/nwx116)
- Jiao, C.-L., Zhu, L., Zhao, E.-g., & Zhang, J. 2025, arXiv e-prints, arXiv:2510.26111, <https://arxiv.org/abs/2510.26111>
- Kaisig, M., Tajima, T., & Lovelace, R. V. E. 1992, *ApJ*, 386, 83, doi: [10.1086/170994](https://doi.org/10.1086/170994)
- Kang, H. D., Perna, R., Lazzati, D., & Wang, Y.-H. 2025, *The Open Journal of Astrophysics*, 8, 23, doi: [10.33232/001c.131902](https://doi.org/10.33232/001c.131902)
- Kato, S., Fukue, J., & Mineshige, S. 2008, *Black-Hole Accretion Disks — Towards a New Paradigm —* (Kyoto University Press)
- Kishor Joshi, R., Bhake, A., Banerjee, B., et al. 2025, arXiv e-prints, arXiv:2509.16796, doi: [10.48550/arXiv.2509.16796](https://doi.org/10.48550/arXiv.2509.16796)
- Kitaki, T., Mineshige, S., Ohsuga, K., & Kawashima, T. 2021, *PASJ*, 73, 450, doi: [10.1093/pasj/psab011](https://doi.org/10.1093/pasj/psab011)
- Kocsis, B., Yunes, N., & Loeb, A. 2011, *PhRvD*, 84, 024032, doi: [10.1103/PhysRevD.84.024032](https://doi.org/10.1103/PhysRevD.84.024032)

- Lazzati, D., Perna, R., Gompertz, B. P., & Levan, A. J. 2023, *ApJL*, 950, L20, doi: [10.3847/2041-8213/acd18c](https://doi.org/10.3847/2041-8213/acd18c)
- Levan, A. J., Malesani, D. B., Gompertz, B. P., et al. 2023, *Nature Astronomy*, 7, 976, doi: [10.1038/s41550-023-01998-8](https://doi.org/10.1038/s41550-023-01998-8)
- Li, F.-L., Liu, Y., Fan, X., et al. 2023, *ApJ*, 950, 161, doi: [10.3847/1538-4357/acd2d1](https://doi.org/10.3847/1538-4357/acd2d1)
- Li, Y.-J., Wang, Y.-Z., Tang, S.-P., & Fan, Y.-Z. 2025, arXiv e-prints, arXiv:2509.23897, doi: [10.48550/arXiv.2509.23897](https://doi.org/10.48550/arXiv.2509.23897)
- Liu, J.-R., Feng, H., & Wang, J.-M. 2025a, arXiv e-prints, arXiv:2509.21958, doi: [10.48550/arXiv.2509.21958](https://doi.org/10.48550/arXiv.2509.21958)
- Liu, J.-R., Wang, Y.-L., & Wang, J.-M. 2024, *ApJ*, 969, 37, doi: [10.3847/1538-4357/ad463a](https://doi.org/10.3847/1538-4357/ad463a)
- Liu, J.-R., Wang, J.-M., Fermi-LAT Collaboration, et al. 2025b, *Nature Astronomy*, 9, 1086, doi: [10.1038/s41550-025-02538-2](https://doi.org/10.1038/s41550-025-02538-2)
- Luo, J., Chen, L.-S., Duan, H.-Z., et al. 2016, *Classical and Quantum Gravity*, 33, 035010, doi: [10.1088/0264-9381/33/3/035010](https://doi.org/10.1088/0264-9381/33/3/035010)
- Luo, Y., & Wang, J.-M. 2025, *MNRAS*, 540, 2413, doi: [10.1093/mnras/staf841](https://doi.org/10.1093/mnras/staf841)
- Lynden-Bell, D. 1969, *Nature*, 223, 690, doi: [10.1038/223690a0](https://doi.org/10.1038/223690a0)
- Lynden-Bell, D., & Pringle, J. E. 1974, *MNRAS*, 168, 603, doi: [10.1093/mnras/168.3.603](https://doi.org/10.1093/mnras/168.3.603)
- Marshall, M. D., Avara, M. J., & McKinney, J. C. 2018, *MNRAS*, 478, 1837, doi: [10.1093/mnras/sty1184](https://doi.org/10.1093/mnras/sty1184)
- McKernan, B., Ford, K. E. S., Cook, H. E., et al. 2025, *ApJ*, 990, 217, doi: [10.3847/1538-4357/adf114](https://doi.org/10.3847/1538-4357/adf114)
- Meier, D. L. 2012, *Black Hole Astrophysics: The Engine Paradigm*, doi: [10.1007/978-3-642-01936-4](https://doi.org/10.1007/978-3-642-01936-4)
- Mishra, B., Begelman, M. C., Armitage, P. J., & Simon, J. B. 2020, *MNRAS*, 492, 1855, doi: [10.1093/mnras/stz3572](https://doi.org/10.1093/mnras/stz3572)
- Moranchel-Basurto, A., Sánchez-Salcedo, F. J., Chametla, R. O., & Velázquez, P. F. 2021, *ApJ*, 906, 15, doi: [10.3847/1538-4357/abca88](https://doi.org/10.3847/1538-4357/abca88)
- Peng, P., & Chen, X. 2021, *MNRAS*, 505, 1324, doi: [10.1093/mnras/stab1419](https://doi.org/10.1093/mnras/stab1419)
- Postiglione, J., Ford, K. E. S., Best, H., McKernan, B., & O'Dowd, M. 2025, *ApJ*, 991, 161, doi: [10.3847/1538-4357/adfa0c](https://doi.org/10.3847/1538-4357/adfa0c)
- Rowan, C., Whitehead, H., Fabj, G., et al. 2025, *MNRAS*, 543, 132, doi: [10.1093/mnras/staf1449](https://doi.org/10.1093/mnras/staf1449)
- Rozyczka, M., Bodenheimer, P., & Lin, D. N. C. 1995, *MNRAS*, 276, 597, doi: [10.1093/mnras/276.2.597](https://doi.org/10.1093/mnras/276.2.597)
- Salpeter, E. E. 1964, *ApJ*, 140, 796, doi: [10.1086/147973](https://doi.org/10.1086/147973)
- Samsing, J., Hendriks, K., Zwick, L., D'Orazio, D. J., & Liu, B. 2025, *ApJ*, 990, 211, doi: [10.3847/1538-4357/ad9f3d](https://doi.org/10.3847/1538-4357/ad9f3d)
- Shakura, N. I., & Sunyaev, R. A. 1973, *A&A*, 24, 337
- She, J.-Z., Liu, T., Huang, B.-Q., et al. 2025, *ApJ*, 990, 17, doi: [10.3847/1538-4357/adefe6](https://doi.org/10.3847/1538-4357/adefe6)
- Sun, H., Li, Y.-P., Pan, Z., & Yang, H. 2025, arXiv e-prints, arXiv:2509.00469, doi: [10.48550/arXiv.2509.00469](https://doi.org/10.48550/arXiv.2509.00469)
- Tagawa, H., Kimura, S. S., Haiman, Z., Perna, R., & Bartos, I. 2023a, *ApJ*, 950, 13, doi: [10.3847/1538-4357/acc4bb](https://doi.org/10.3847/1538-4357/acc4bb)
- . 2023b, *ApJL*, 946, L3, doi: [10.3847/2041-8213/acc103](https://doi.org/10.3847/2041-8213/acc103)
- Tagawa, H., Kimura, S. S., Haiman, Z., et al. 2022, *ApJ*, 927, 41, doi: [10.3847/1538-4357/ac45f8](https://doi.org/10.3847/1538-4357/ac45f8)
- Takeuchi, S., Mineshige, S., & Ohsuga, K. 2009, *PASJ*, 61, 783, doi: [10.1093/pasj/61.4.783](https://doi.org/10.1093/pasj/61.4.783)
- The LIGO Scientific Collaboration, the Virgo Collaboration, the KAGRA Collaboration, et al. 2025, arXiv e-prints, arXiv:2507.08219, doi: [10.48550/arXiv.2507.08219](https://doi.org/10.48550/arXiv.2507.08219)
- Trani, A. A., & Di Cintio, P. 2025, arXiv e-prints, arXiv:2506.02173, doi: [10.48550/arXiv.2506.02173](https://doi.org/10.48550/arXiv.2506.02173)
- Vaccaro, M. P. 2025, arXiv e-prints, arXiv:2508.15337, doi: [10.48550/arXiv.2508.15337](https://doi.org/10.48550/arXiv.2508.15337)
- Vaccaro, M. P., Seif, Y., & Mapelli, M. 2025, arXiv e-prints, arXiv:2508.03637, doi: [10.48550/arXiv.2508.03637](https://doi.org/10.48550/arXiv.2508.03637)
- Wang, J.-M., Liu, J.-R., Ho, L. C., & Du, P. 2021a, *ApJL*, 911, L14, doi: [10.3847/2041-8213/abee81](https://doi.org/10.3847/2041-8213/abee81)
- Wang, J.-M., Liu, J.-R., Ho, L. C., Li, Y.-R., & Du, P. 2021b, *ApJL*, 916, L17, doi: [10.3847/2041-8213/ac0b46](https://doi.org/10.3847/2041-8213/ac0b46)
- Wang, J.-M., Liu, J.-R., Li, Y.-R., et al. 2023a, *ApJL*, 958, L40, doi: [10.3847/2041-8213/ad0bd9](https://doi.org/10.3847/2041-8213/ad0bd9)
- Wang, J.-M., Yan, C.-S., Gao, H.-Q., et al. 2010, *ApJL*, 719, L148, doi: [10.1088/2041-8205/719/2/L148](https://doi.org/10.1088/2041-8205/719/2/L148)
- Wang, J.-M., Yan, C.-S., Li, Y.-R., et al. 2009, *ApJL*, 701, L7, doi: [10.1088/0004-637X/701/1/L7](https://doi.org/10.1088/0004-637X/701/1/L7)
- Wang, J.-M., Zhai, S., Li, Y.-R., et al. 2023b, *ApJ*, 954, 84, doi: [10.3847/1538-4357/acdf48](https://doi.org/10.3847/1538-4357/acdf48)
- Wang, J.-M., Hu, C., Chen, Y.-J., et al. 2025a, arXiv e-prints, arXiv:2511.07716, doi: [10.48550/arXiv.2511.07716](https://doi.org/10.48550/arXiv.2511.07716)
- Wang, J.-M., Wang, Y.-L., Chen, Y.-J., et al. 2025b, arXiv e-prints, arXiv:2511.09278, doi: [10.48550/arXiv.2511.09278](https://doi.org/10.48550/arXiv.2511.09278)
- Wang, M., Ma, Y., Li, H., et al. 2025c, *ApJ*, 983, 114, doi: [10.3847/1538-4357/adbf8e](https://doi.org/10.3847/1538-4357/adbf8e)
- Wang, M., Wu, Q., & Ma, Y. 2025d, arXiv e-prints, arXiv:2507.07715, doi: [10.48550/arXiv.2507.07715](https://doi.org/10.48550/arXiv.2507.07715)
- Weaver, R., McCray, R., Castor, J., Shapiro, P., & Moore, R. 1977, *ApJ*, 218, 377, doi: [10.1086/155692](https://doi.org/10.1086/155692)
- Whitehead, H., Rowan, C., & Kocsis, B. 2025a, *MNRAS*, doi: [10.1093/mnras/staf1686](https://doi.org/10.1093/mnras/staf1686)
- . 2025b, *MNRAS*, 542, 1033, doi: [10.1093/mnras/staf1271](https://doi.org/10.1093/mnras/staf1271)
- Xing, J.-T., Liu, T., Huang, B.-Q., & Sun, M. 2025, *ApJ*, 991, 167, doi: [10.3847/1538-4357/adff71](https://doi.org/10.3847/1538-4357/adff71)
- Xu, Z.-H. 2025, *Research in Astronomy and Astrophysics*, 25, 115013, doi: [10.1088/1674-4527/adfeb9](https://doi.org/10.1088/1674-4527/adfeb9)
- Xue, L., Tagawa, H., Haiman, Z., & Bartos, I. 2025, *PhRvD*, 112, 063034, doi: [10.1103/5m1n-9h9v](https://doi.org/10.1103/5m1n-9h9v)
- Yan, C.-S., & Wang, J.-M. 2010, *ApJ*, 725, 2359, doi: [10.1088/0004-637X/725/2/2359](https://doi.org/10.1088/0004-637X/725/2/2359)

- Yang, S.-C., Han, W.-B., Tagawa, H., Li, S., & Zhang, C. 2025, ApJL, 988, L41, doi: [10.3847/2041-8213/adeaad](https://doi.org/10.3847/2041-8213/adeaad)
- Yang, Y., Bartos, I., Haiman, Z., et al. 2019, ApJ, 876, 122, doi: [10.3847/1538-4357/ab16e3](https://doi.org/10.3847/1538-4357/ab16e3)
- Yuan, H.-Y., & Lei, W.-H. 2025, ApJ, 987, 167, doi: [10.3847/1538-4357/addbe4](https://doi.org/10.3847/1538-4357/addbe4)
- Zeldovich, Y. B. 1964, Soviet Physics Doklady, 9, 195
- Zhai, S., Wang, J.-M., Li, Y.-R., Guo, W.-J., & Zhao, G. 2025, arXiv e-prints, arXiv:2511.16119, doi: [10.48550/arXiv.2511.16119](https://doi.org/10.48550/arXiv.2511.16119)
- Zhang, H.-H., Zhu, J.-P., & Yu, Y.-W. 2024, ApJ, 976, 63, doi: [10.3847/1538-4357/ad8139](https://doi.org/10.3847/1538-4357/ad8139)
- Zhang, L., Stone, J. M., White, C. J., et al. 2025a, arXiv e-prints, arXiv:2509.10638, doi: [10.48550/arXiv.2509.10638](https://doi.org/10.48550/arXiv.2509.10638)
- Zhang, S.-R., Wang, Y., Yuan, Y.-F., et al. 2025b, arXiv e-prints, arXiv:2505.10395, doi: [10.48550/arXiv.2505.10395](https://doi.org/10.48550/arXiv.2505.10395)
- Zhao, Z. Y., Chen, K., Wang, F. Y., & Dai, Z.-G. 2024, MNRAS, 530, 1644, doi: [10.1093/mnras/stae957](https://doi.org/10.1093/mnras/stae957)
- Zhou, S., Sun, M., Liu, T., et al. 2024, ApJL, 966, L9, doi: [10.3847/2041-8213/ad3c3f](https://doi.org/10.3847/2041-8213/ad3c3f)
- Zhou, Y., Feng, H., Ho, L. C., & Yao, Y. 2019, ApJ, 871, 115, doi: [10.3847/1538-4357/aaf724](https://doi.org/10.3847/1538-4357/aaf724)